

NASA TECHNICAL NOTE



NASA TN D-5142

C.1

NASA TN D-5142



LOAN COPY: RETURN TO
AFWL (WLOL)
KIRTLAND AFB, N MEX

**OCEAN CURRENT AND SEA SURFACE
TEMPERATURE OBSERVATIONS
FROM METEOROLOGICAL SATELLITES**

*by Guenter Warnecke, Larry M. McMillin, and Lewis J. Allison
Goddard Space Flight Center
Greenbelt, Md.*

National Aeronautics and Space Administration

ERRATUM

*Completed
23 Aug 70
SW*


NASA Technical Note D-5142

OCEAN CURRENT AND SEA SURFACE TEMPERATURE OBSERVATIONS FROM METEOROLOGICAL SATELLITES

Guenter Warnecke, Larry M. McMillin, and Lewis J. Allison

November 1969

The captions of Figures 6 and 7 were interchanged. The corrected versions appear below.





0131849

NASA TN D-5142

OCEAN CURRENT AND SEA SURFACE TEMPERATURE
OBSERVATIONS FROM METEOROLOGICAL SATELLITES

By Guenter Warnecke, Larry M. McMillin, and Lewis J. Allison

Goddard Space Flight Center
Greenbelt, Md.

NATIONAL AERONAUTICS AND SPACE ADMINISTRATION

For sale by the Clearinghouse for Federal Scientific and Technical Information
Springfield, Virginia 22151 - CFSTI price \$3.00

ABSTRACT

Television and infrared sensing techniques utilized by meteorological satellites provide a very useful tool for oceanographic research.

Satellite television pictures of cloud patterns overlying thermally different oceanic boundaries reveal significant features of sea surface temperature distribution. Nimbus II High Resolution Infrared Radiometer (HRIR) data which is sensitive in the 3.4 to 4.2 micron window were analyzed over several oceanic regions. Quantitative sea surface temperatures within an accuracy of $\pm 2^{\circ}\text{K}$ were derived from nighttime satellite radiance measurements in the absence of clouds. Comparisons with observations from low flying radiometer-equipped aircraft confirmed good absolute sea surface temperature measurements from the satellite radiometer if 3° to 4°K corrections for atmospheric attenuation and other losses were applied. Sea surface temperature discontinuities such as the North Wall of the Gulf Stream have been located consistently within 10 kilometers of the positions indicated by the airplane radiation data. With present techniques, primarily designed for meteorological purposes, the Gulf Stream boundary has been seen, at least in significant parts in about 50 out of 175 days. Similar results have also been obtained in analyses of the Agulhas Current boundary, the boundary between the Brazil and Falkland Currents and the Kurishio - Oyashio mixing region. These satellite radiation observations suggest that the Brazil-Falkland Current boundary which is associated with a surface temperature discontinuity is as sharp and strong as the Gulf Stream North Wall. The Agulhas Current exhibits a similar temperature discontinuity along its western boundary, which separates it from the Benguela Current surface waters.

Daytime observations within the 3.4 to 4.2 micron window have also shown qualitatively the location of major current boundaries.

For detailed oceanographic research work in the future, a higher spatial resolution and a shift to the 10 to 11 micron region is desirable. Simultaneous window channel observations with a visible channel (0.55 to 0.75μ) would be necessary to delineate and eliminate cloud contaminated areas within the field of view of the radiometer.

CONTENTS

Abstract.	ii
INTRODUCTION	1
INFERENCE OF SEA SURFACE TEMPERATURE PATTERNS FROM SATELLITE CLOUD OBSERVATIONS.	2
THEORY OF SEA SURFACE TEMPERATURE MEASUREMENTS FROM SPACE IN THE INFRARED	6
Interpretation of the Radiative Transfer Equation	6
Definition of Sea Surface	7
Atmospheric Attenuation.	7
Cloud Interference.	8
Daytime Observations.	8
INFRARED RADIATION EXPERIMENTS.	9
Medium Resolution Radiometer Measurements	9
High Resolution Radiometer Measurements	9
The Nimbus II HRIR Experiment.	10
SEA SURFACE TEMPERATURE PATTERNS DERIVED FROM NIMBUS II OBSERVATIONS	17
Daytime Infrared Observations.	19
Nighttime Infrared Observations.	24
CONCLUSIONS	41
ACKNOWLEDGMENTS	44
References.	44

OCEAN CURRENT AND SEA SURFACE TEMPERATURE OBSERVATIONS FROM METEOROLOGICAL SATELLITES

by

Guenter Warnecke,* Larry M. McMillin,[†] and Lewis J. Allison
Goddard Space Flight Center

INTRODUCTION

Polar-orbiting and geostationary satellites are valuable observational tools in geophysics because of their ability to scan the distribution of physical properties in various scales synoptically over large areas or over the entire globe in a reasonably short time. In probing the earth's surface and lower atmosphere from space, the remote sensing of electromagnetic radiation is of primary importance. The limited penetration of electromagnetic waves through water restricts oceanographic applications to relatively shallow layers or even to the immediate surface only, depending on the spectral region.

Although no specific oceanographic experiments have yet been performed from spacecraft, airborne oceanographic observations from airplanes as well as from manned spaceflights and unmanned meteorological satellites indicate a large potential for future oceanographic research and application. In the visible part of the spectrum, visual and photographic observations from airplanes and manned spacecraft have shown evidence that remote aerial observations can contribute considerably to near-coast and open-sea research (Ewing, 1965; National Council on Marine Resources and Engineering Development, 1967). A number of experiments have been performed in the infrared to measure, for meteorological purposes, the radiation of the earth-atmosphere system in various spectral regions (Bandein, 1968). In an atmospheric "window," i.e., in a spectral region where gaseous absorption does not exist (ideal case) or is at a pronounced minimum (natural case), according to radiative transfer theory, measurements of the outgoing thermal radiance can be interpreted in terms of the temperature of an opaque surface (e.g. land, water, thick clouds, etc.) provided that the emissivity of the surface is known and the surface fills the field of view of the radiometer. Therefore, under clear-sky conditions, radiometric measurements in a spectral window region taken at satellite altitudes should provide quantitative information on sea surface temperature. Because of the quasipolar orbits of present weather satellites and the scanning mode of the radiometers used, global mapping of sea surface temperatures should become possible.

*On leave from the Freie Universität Berlin, Germany, as a NAS-NRC Senior Post-doctoral Resident Research Associate with the Planetary Radiations Branch, Goddard Space Flight Center.

[†]Allied Research Inc., Concord, Mass.; present affiliation, Department of Earth Sciences, Iowa State University, Ames, Iowa.

Infrared techniques in measuring sea surface temperature have been applied before from ship-board and airplanes (J. Clark, 1964; Wilkerson, 1966), and a detailed discussion of the physics of aircraft measurements has been given by H. L. Clark (1967). However, only sporadic measurements are possible from a ship, and even airborne scanning radiometers can only cover very limited areas that are restricted by the limited flight altitude, operational range of the aircraft, and frequency of flights. Thus, a polar-orbiting satellite with its ability of repeatedly mapping the entire globe in 12-hour intervals suggests an ideal means of monitoring sea surface temperature distributions from space.

In this report, the remote detection of ocean currents and sea surface temperature patterns will be discussed. A brief description of the theoretical background of sea surface temperature measurements from space will be given, and the feasibility of this method will be explored by means of experimental results mainly from measurements aboard the Nimbus II satellite.

INFERENCE OF SEA SURFACE TEMPERATURE PATTERNS FROM SATELLITE CLOUD OBSERVATIONS

Slight color differences along the boundary between ocean currents have been observed from aircraft and documented in color photographs; however, no multispectral color techniques have been developed for spacecraft utilization. Present photographic (television) techniques of observation from satellites designed merely for meteorological purposes do not have the spatial and spectral resolution necessary for such a purpose. Thus, at present only inferences of differential sea surface temperature from televised cloud features are possible. This method is, however, restricted to certain meteorological conditions.

The cloud patterns seen in television pictures are determined mainly by the structural and dynamical conditions within the atmosphere itself. The influence of surface properties on the cloud structure is extremely variable in character, space, and time. It can be recognized easily in the case of temperature differences between land and the oceans. However, over the ocean, with its comparably small horizontal temperature differences, the surface effect usually appears overridden by the effect of internal atmospheric processes on the cloud structure. In the case of rather homogeneous horizontal conditions and fairly weak large-scale dynamic activity in the atmosphere, sea surface temperature characteristics can be reflected in the cloud patterns, as has been shown by Warnecke et al. (1968) and the National Council on Marine Resources and Engineering Development (1967). An excellent example is presented in Figure 1.

On April 10, 1967, the satellite ATS-II made a remarkable TV photograph of the eastern tropical Pacific Ocean. In this photograph, the position of the Humboldt (or Peru) Current and its western continuation, the South Equatorial Current, is recognizable in the cloud pattern by a distinct zone of clear skies stretching from the Peruvian coast westward across the Galapagos Archipelago and along the equator. This clear zone seemingly follows the historical course of the Humboldt

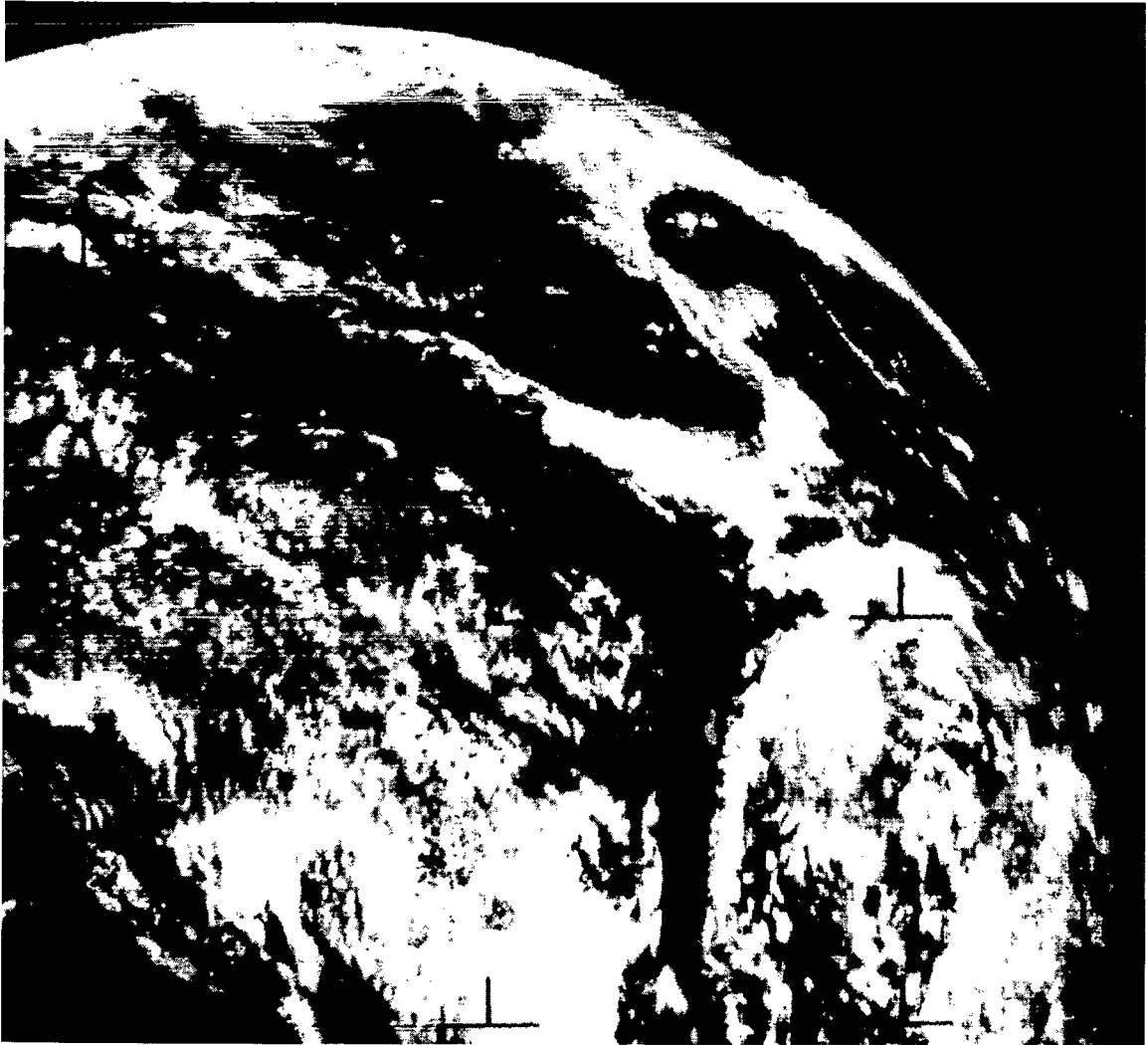


Figure 1—ATS-II photograph taken on April 10, 1967, 1855 GMT, over the eastern Pacific Ocean. South America in the lower right is outlined by heavy cloudiness. The Peruvian coast is under clear skies; the Humboldt Current is marked by the extended band of no or little cloudiness through the center of the picture. Central America, the Gulf Coast, and southern Baja California are visible in the upper center portions.

Current, which is a pronounced cold water stream that departs from the South American coast at Punta Negra, Peru. The current is, on the average, 2 to 5°K colder than the surrounding sea regions. This temperature difference seems to be quite sufficient to suppress the formation of convective cloudiness which is, in this case, present over all the surrounding warm water areas. In some portions, the boundaries of the cold water are even delineated by pronounced cloud bands that suggest the existence of a superimposed meso-scale thermal circulation between the cold and warm water regions, similar to the land-sea-breeze phenomenon.

In the series of photographs provided since November 1967 by the ATS-III satellite, which was stationary over the equator near South America, the outlines of the Humboldt Current are a pronounced phenomenon in almost every picture. Two examples (Figures 2 and 3) were selected in order to demonstrate the persistence of the exhibited cloud patterns from day to day. In both figures, the cold water of the Humboldt Current obviously suppresses the extended convective cloudiness present elsewhere; again, distinct cloud bands representing the upward branch of the induced local circulation accentuate at least parts of the current boundary.

Depending on the season and the synoptic weather situation, the cold water area is not always free of clouds. Middle and high-layer cloud systems are influenced less by the thermal differences at the underlying surface than are low-level and convective cloud systems. However, even in many cloudy cases, structural changes in the cloud patterns are very obvious over the Humboldt Current and help depict the location of the boundaries as is illustrated by Figure 4. In this case, large parts of the Humboldt Current are covered by mostly stratified clouds; nevertheless, the western current boundary can be recognized easily by a distinct difference in cloud density and even by a narrow break along the current boundary. This break can be understood as a reflection

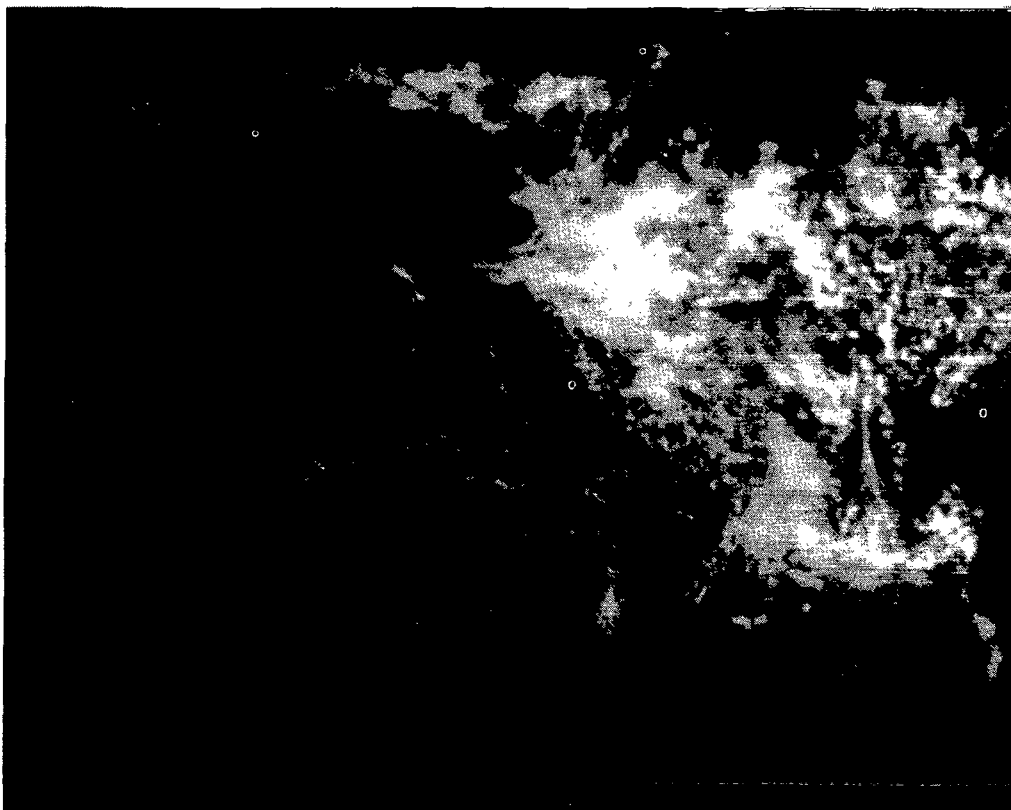


Figure 2—Section of ATS-III photograph (IDCS) taken on March 11, 1968, 1622 GMT, showing South America and the eastern South Pacific Ocean. The largest parts of the continent are cloud-covered; the coasts of Chile and Peru are visible under clear skies that extend inland from the clear region of the Humboldt Current.



Figure 3—Section of an ATS-III photograph (IDCS) taken on March 12, 1968, 1659 GMT, showing South America and the eastern South Pacific Ocean. The Humboldt Current is demarked by the extended band of clear skies through the center of the picture.

of the subsiding branch of the local atmospheric circulation across the sea surface temperature discontinuity.

From the foregoing discussion, it can be concluded that present satellite photography can provide information useful in detecting pronounced sea surface temperature discontinuities, essentially along contrasting ocean surface currents. The location must be inferred visually from characteristic modifications of existing cloud patterns as caused by differential sea surface temperature patterns and the concurrently induced local vertical circulations in the lower atmosphere. However, since the cloud features merely reflect these induced lower tropospheric local circulations rather than the sea surface temperature itself, the locations of the ocean current boundary and the cloud boundary need not coincide because of the width of the horizontal air motion across the current boundary. Therefore, an allowance for a displacement of approximately 10 kilometers toward the warmer water seems to be adequate. Also, a larger-scale atmospheric flow pattern might be superimposed on the local circulation, thus resulting in an additional displacement of the cloud boundary in a direction dependent on the superimposed wind field. The average distance between a distinct cloud boundary parallel to the Gulf Stream north wall from the sea surface temperature discontinuity, observed near the center of a large atmospheric high pressure system and reported

earlier by Warnecke, et al. (1968), was approximately 20 to 40 kilometers. Additionally, movies from ATS-III time-lapse photographs taken over full daytime periods indicate a slight, but pronounced, diurnal variation of the cold patterns over the Humboldt Current or along its boundary. These effects may complicate the locating of an ocean current boundary accurately by its influence on cloud patterns, but no detailed and quantitative investigation of this problem has been accomplished.

THEORY OF SEA SURFACE TEMPERATURE MEASUREMENTS FROM SPACE IN THE INFRARED

Interpretation of the Radiative Transfer Equation

The thermal radiation leaving the earth's atmosphere at satellite altitude and measured through a filter system can be described by the radiative transfer equation

$$N = \frac{1}{\pi} \int_{\lambda_1}^{\lambda_2} \Phi(\lambda) \tau_s(\lambda) \epsilon_s(\lambda) B(\lambda, T_s) d\lambda + \frac{1}{\pi} \int_{\lambda_1}^{\lambda_2} \int_{h=0}^{h_\infty} \Phi(\lambda) \frac{\partial \tau(\lambda, h)}{\partial h} B[\lambda, T(h)] dh d\lambda, (1)$$

where

N is the detected radiance,

λ is the wavelength,

$\Phi(\lambda)$ is the filter function [$\Phi(\lambda) = 0$ outside the interval λ_1, λ_2],

$\tau(\lambda)$ is the transmissivity from a height h to the satellite at height h_∞ ,

$\tau_s(\lambda)$ is the transmissivity from the radiating surface to the satellite,

$\epsilon_s(\lambda)$ is the emissivity of the radiating surface,

$B(\lambda, T)$ is the Planck function,

T is the absolute temperature, and

T_s is the temperature of the radiating surface.



Figure 4—Section of an ATS-III photograph (MSSC camera) taken on May 31, 1968, 1614 GMT, showing South America and the South Pacific Ocean. The coastal regions of Chile and Peru are visible under clear skies. The southern parts of the Humboldt Current are characterized in this picture by clear skies, while clouds cover the northern parts of the ocean current. The underlying sea surface temperature distribution is, however, reflected in the cloud structure over the cold water current.

The first term on the right side of this equation describes the contribution of an opaque surface, both solid and liquid (such as the earth, ocean, thick clouds, etc.), to the recorded radiance; the second term describes the radiation originating from the gaseous compounds of the atmosphere and optically tenuous constituents such as thin clouds, and dust.

In an ideal atmospheric "window" (transmissivity $\tau = \tau_s = 1$) Equation 1 reduces to

$$N_w = \frac{1}{\pi} \int_{\lambda_1}^{\lambda_2} \Phi(\lambda) \epsilon_s(\lambda) B(\lambda, T_s) d\lambda. \quad (2)$$

With $\Phi(\lambda)$ known, the measured radiance from a water surface N_w depends only on $\epsilon_s(\lambda)$ and T_s . The emissivity of water is well known and varies little (between 0.90 and 0.99, depending on wavelength and view angle) in the presently-used infrared windows (Bramson et al., 1964). For most meteorological purposes, such as detecting clouds, black body radiation ($\epsilon = 1.0$) can be assumed without introducing a large error. Thus, N_w depends on only one unknown variable—i.e., the temperature T_s of the radiating surface. In the case of clear skies and over water surfaces, T_s closely represents approximately the sea surface temperature. If absolute temperature values, accurate within a few degrees Kelvin are required, corrections for $\epsilon < 1.0$ become necessary, at least on the basis of an average emissivity.

Definition of Sea Surface

On the basis of Kirchhoff's Law, the high emissivity of liquid water in the infrared also means that its absorptivity is high. A layer of less than 1 mm of water is opaque for infrared radiation from 8 to 14 microns; 98 percent of the absorption occurs even in the first 0.1-mm layer (Ewing and McAlister, 1960). This means that the observed infrared radiation emerges from the very top of the air-water interface, the "microsurface" where transfer processes (evaporation, reflection) take place and also microsurface properties (protein monolayer, dust, and oil films) are significant. Conventionally, sea surface temperature is defined as a mean temperature of a well-mixed layer at least several decimeters deep in reasonable accordance with the nature of conventional sea surface temperature observations ("bucket" or "intake" thermometric measurements). However, experiments have shown (Ewing and McAlister, 1960) that the microsurface is approximately 0.6°K colder than the layer immediately underneath (15-cm depth). It has also been observed that the microsurface is remarkably stable; it regenerates within tens of seconds after being disturbed by intense stirring or breaking of waves. Thus, under clear-sky conditions, radiometric measurements of sea surface temperature generally should be approximately 0.6°K lower than conventional measurements.

Atmospheric Attenuation

In reality, no atmospheric "window" is absolutely clean. Therefore, exact considerations must account for absorption of infrared radiation at least by the predominant tri-atomic atmospheric gases—water vapor, ozone, and carbon dioxide; then the complete radiative transfer equation (Equation 1) will apply. According to Equation 1, absorption (and reradiation) vary with the gas distribution $\partial\tau/\partial h$ and the gas temperature $T(h)$ along the optical path; also absorption will vary

greatly with wavelength, depending on the actual location and extension of the absorption bands within the chosen filter range. Also, depending on the spatial distributions of the individual gases, their contributions to the detected outgoing radiance at satellite altitudes will peak in different layers in the atmosphere. Water vapor is the most important absorber and the most difficult one to handle because of its large variability in space and time in the atmosphere. Nevertheless, proper corrections must be applied to the satellite measurements in order to derive correct sea surface temperatures. These corrections will be discussed later in conjunction with the individual experiments.

Cloud Interference

A unique interpretation of the radiance measurements from a satellite in terms of sea surface temperature involves the assumption of a homogeneous, nontransparent target that fills the radiometer field of view. Because of the generally observed, vertical temperature decrease in the troposphere, any cloud "seen" by the radiometer will reduce the detected radiance and result in lower target temperature. This is true for opaque clouds filling a part of the field of view as well as for partly transparent clouds such as thin cirrus. The probability of having the field of view undisturbed by clouds increases with a decrease in the size of the field of view. Reducing the field of view, however, is limited by the sensitivity of the sensor because the signal strength decreases with a decreasing field of view; thus the signal-to-noise ratio becomes more and more unfavorable. Also the data volume increases with a decreasing field of view if total areal coverage is maintained, thus imposing greater data reduction requirements. In order to determine whether clouds contaminate the radiation measurements, simultaneous cloud photographs from the same satellite will be a valuable source of information for proper interpretation of the radiation data.

Daytime Observations

The foregoing considerations of radiative transfer hold for thermal radiation only. These conditions are fully realistic, however, only on the night side of the earth. During daytime, they are still valid for infrared wavelengths beyond 5 microns. In the near infrared, 0.8 micron to 4 microns, reflected sunlight is superimposed on the thermal radiation, and the term

$$R_s(\lambda) = \frac{1}{\pi} \int_{\lambda_1}^{\lambda_2} \Phi(\lambda) r_s(\lambda) H(\lambda) \cos z \, d\lambda$$

must be added on the right side of the radiative transfer equation (Equation 1). This term represents the reflected solar radiation seen in the field of view and through the radiometer filter $\Phi(\lambda)$; $H(\lambda)$ is the spectral solar irradiance; $H(\lambda) \cdot \cos z$ the spectral irradiance on the horizontal reflecting surface, where z is the zenith angle of the sun; and r_s is the reflectivity of the viewed surface. Isotropic reflection is assumed.

In a perfect atmospheric window ($\tau = 1.0$), the radiative transfer equation then will apply in the form

$$N_w^* = \frac{1}{\pi} \int_{\lambda_1}^{\lambda_2} \Phi(\lambda) \epsilon_s(\lambda) B(\lambda, T_s) d\lambda + \frac{1}{\pi} \int_{\lambda_1}^{\lambda_2} \Phi(\lambda) r_s(\lambda) H(\lambda) \cos z d\lambda.$$

The radiometer, however, is calibrated in accordance with the thermal radiation of a black body of known temperature T :

$$N_w^* = \frac{1}{\pi} \int_{\lambda_1}^{\lambda_2} \Phi(\lambda) B(\lambda, T_{BB}) d\lambda.$$

Thus, for a natural target, the simple assumption of T_{BB} representing T_s is no longer valid since with $r_s(\lambda)$ a new variable is introduced. Also, taking into account the residual atmospheric absorption within the window, $H(\lambda)$ will also become variable because of the variations in atmospheric transmission. Under these conditions, deriving sea surface temperature accurately from daytime radiometric measurements under clear sky conditions becomes very difficult. However, it will be shown later that certain characteristics of sea surface temperature patterns such as sharp temperature discontinuities at ocean current boundaries are recognizable in the near-infrared daytime observations.

INFRARED RADIATION EXPERIMENTS

Medium Resolution Radiometer Measurements

Radiometers sensitive in the 8- to 12-micron "window" region were flown on Tiros II, III, IV, and VII. The large spectral range of approximately 4 microns involved an appreciable attenuation of the measurements predominantly by water vapor, but also by atmospheric ozone (9.6-micron band). Because the actual vertical distribution of these gases is known only at certain times and at relatively few places over the globe (i.e., in the vicinity of radiosonde stations which are particularly rare in the oceanic areas), it was necessary to develop correction models (Wark et al., 1962) on the basis of average conditions. These models are satisfactory for most meteorological purposes; however, for oceanographic applications, the uncertainties involved in the correction models are too large to yield reliable information on sea surface temperature. Additionally the 5-degree field of view of the medium resolution infrared radiometer (MRIR) resulted in a scan-spot at the earth's surface at least 60 kilometers in diameter, which is too large for oceanographic requirements.

High Resolution Radiometer Measurements

For the Nimbus satellites, a high resolution infrared radiometer (HRIR) with a 0.5-degree field of view responding in the 3.5- to 4.1-micron window was developed, and it became possible

for the first time (Allison and Kennedy, 1967) to derive certain sea surface temperature features from the Nimbus I measurements. However, the short lifetime of the Nimbus I experiment severely limited the volume of useful data.

The Nimbus II satellite, with an HRIR lifetime of 6 months, furnished a large volume of high quality data that could be explored more intensively for oceanographic applicability. A number of examples and preliminary results have already been published (Nordberg and Samuelson, 1965; Warnecke et al., 1968; Wilkerson, 1967; National Council on Marine Resources and Engineering Development, 1967; La Violette and Chabot, 1968; Rao, 1968; and Greaves et al., 1968). This report summarizes the results of a more systematic investigation.

The Nimbus II HRIR Experiment

The Nimbus II satellite was launched on May 15, 1966 into an earth-oriented, quasi-polar, near-circular, sun-synchronous orbit. Its perigee was 1095 km, the apogee 1179 km, and the orbital inclination angle was 100.3 degrees. The ascending nodes occurred 32 minutes before noon, local mean solar time, and varied in position from day to day; graphs of the orbits are published in catalog form (Nimbus Project, 1966b).

The high resolution infrared radiometer (HRIR) experiment lasted from May 20 through November 15, 1966. The instrument, described in more detail in the Nimbus II User's Guide (Nimbus Project, 1966a), was a single-channel scanning radiometer sensitive in the 3.5- to 4.1-micron window region. Its sensor was a lead selenide (PbSe) photoconductive cell radiatively cooled to approximately 198°K. The radiometer was designed to measure radiance temperatures between 210°K and 330°K with noise-equivalent-temperature differences of 1°K for a 250°K background. In-flight calibration was achieved by viewing alternately space and the spacecraft housing, the temperature of which was monitored during each scan.

Ground calibration of the radiometer in terms of effective radiance

$$N_{eff} = \frac{1}{\pi} \int_0^{\infty} \Phi(\lambda) B(\lambda, T_{BB}) d\lambda$$

was performed against a black body of variable, known temperature. The effective radiance measured from space,

$$N_{eff} = \int_0^{\infty} \Phi(\lambda) N(\lambda) d\lambda ,$$

thus is translatable into "equivalent black body temperature" T_{BB} of a radiating source filling the field of view of the sensor.

Scanning was performed by a mirror rotating perpendicular to the orbital plane at a rate of 44.7 rpm. Because of the field of view, satellite altitude, and satellite motion, continuous mapping was accomplished with contiguous scanning near the subsatellite track but with increasing overlap toward the horizons. The aperture and the height resulted in a rectangular scan spot approximately 8.6 by 9.7 kilometers at the subsatellite point.

Data Display

A continuous reading of the radiometer output in analog form was transmitted from the spacecraft. These data are available in three forms:

1. as a function of satellite time in analog form, as recorded at the ground station,
2. in the form of a playback on photographic film with a superimposed, approximate geographic grid, and
3. as a digitized version of the radiometer data documented on Nimbus meteorological radiation tapes (NMRT) that can be used readily for computer processing, particularly for the production of two-dimensional data display in the form of standard map projections.

The analog data contain the total volume of information. The tremendous data volume and the difficulty of analyzing analog data limit the practical application to selected studies where extreme detail is required.

The photographic display of the analog data is the most convenient one, and a survey catalog of all available filmstrips has been published (Nimbus Project, 1967). For proper location of the data, a computer-processed, approximate geographic grid was superimposed on each filmstrip. The accuracy of the grid is nominally within 2 degrees of great circle arc at the subsatellite point. At the sides of the filmstrip near the horizons, severe distortions occur because of the scanning geometry. This effect and also the fact that an absolute relation between film density and temperature cannot be derived for these contrast-enhanced filmstrips further limit their applicability.

Digitization of the analog data in conjunction with the concurrent orbital and attitude information leads to the mentioned NMR tapes, which represent the most useful data documentation for quantitative work. Mapping programs exist that print the data in standard map projections. The advantages of this form of data display are the presentation of absolute values, the elimination of distortion, and the possibility of automatically composing measurements from consecutive orbits into quasi-synoptic areal maps. However, because of the scanning geometry, either a loss of detail will result from averaging in the center portions of each swath or data gaps will occur at some distance from the subsatellite point where data spacing may be larger than the grid interval. These disadvantages, on the other hand, can be eliminated at least partly by the selection of proper map scales. Experience has shown that for oceanographic purposes a map scale of 1:1 million appears to be most favorable. Automatic contouring or the transformation of the numerical values into easily distinguished color schemes are well proven additional aids for easier recognition of sea surface temperature patterns, while conserving the quantitative information.

Theoretical Data Accuracy and Interpretation

The 3- to 4-micron window is located in the near-infrared. In this spectral region, solar radiation reflected from the surface of the earth and clouds is superimposed on the thermal radiation seen by a downward-looking instrument under daylight conditions. Therefore, the physical relationship between the measured radiance and the temperature of the radiating surface is no longer valid. Consequently, in contrast to measurements in the 8- to 12-micron window, daytime Nimbus HRIR measurements are not applicable for the determination of sea surface temperature, although qualitative information such as the location of sharp sea surface temperature discontinuities can be derived under clear-sky conditions.

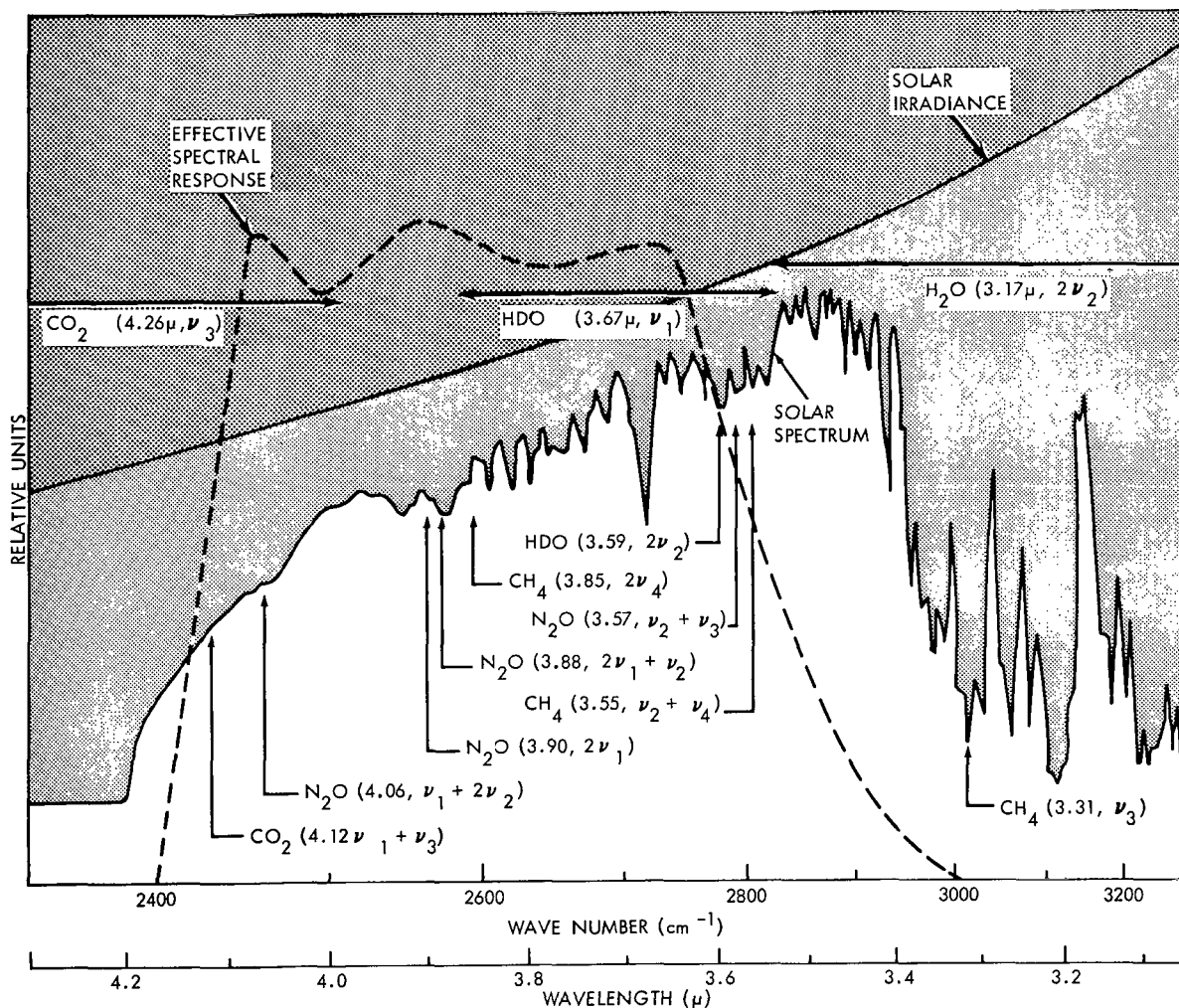


Figure 5—The 4-micron window region. The upper solid curve represents the solar irradiance of a 6000°K black body at the top of the atmosphere, and the lower solid curve an infrared prismatic solar spectrum (Shaw et al., 1951). The darker, shaded area represents the solar energy loss, mainly caused by molecular absorption, in the earth's atmosphere. The horizontal lines indicate approximately the regions of absorption due to the major absorbing gases. The vertical lines indicate the center of absorption band due to major constituents (Goody, 1964). The dashed curve is the effective spectral response of the HRIR, (after Kunde, 1965)

The theoretical relationship between the measured nighttime equivalent black body temperature and surface temperature measured by the Nimbus high resolution infrared radiometer as described for the Nimbus I instrument by Kunde (1965) is also valid for the almost identical Nimbus II HRIR.

As indicated in Figure 5, residual molecular absorption in the 3- to 4-micron region is caused by water vapor (H_2O), carbon dioxide (CO_2), methane (CH_4), and nitrous oxide (N_2O). The absorption by the minor constituents CH_4 and N_2O is negligible compared to the effect of CO_2 and water vapor, the spectral distribution of which is quantitatively shown in Figure 6.

The results of computations of water vapor and carbon dioxide absorption for a number of model atmospheres and based on radiative transfer theory are reproduced in Figure 7. Absorption by CH_4 and N_2O has been neglected and the emission and scattering by aerosols have not been taken into account. However, the results can be considered very close to natural conditions.

From Figure 7 it follows that for zenith angles of the measured beam of less than 50 degrees, even in an extreme moist atmosphere (4.7-cm precipitable water content), the necessary correction

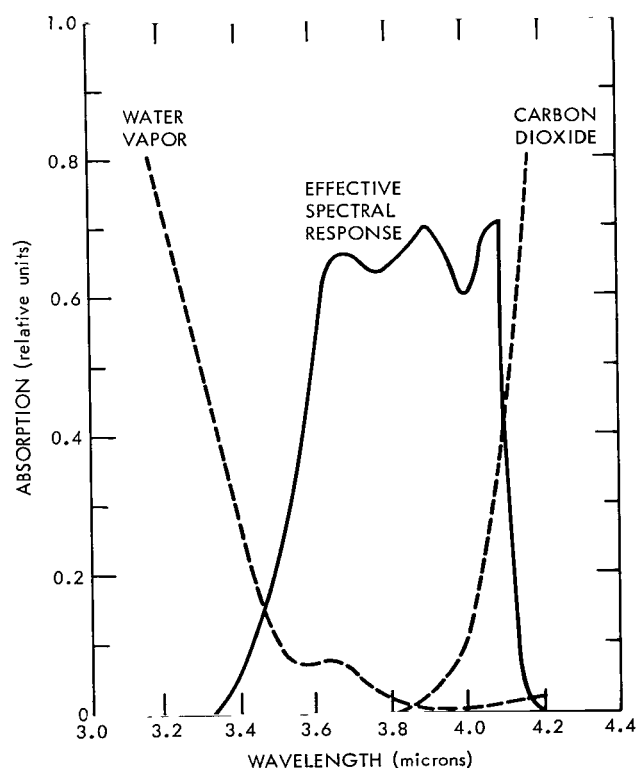


Figure 7—The fractional contribution to the total outgoing effective radiance from each atmospheric layer. The assumed conditions are noted in the upper lefthand corner (after Kunde, 1965).

to the measured equivalent black body temperature does not exceed 4°K. On the average, a correction of +1 to 2°K will be sufficient. For higher accuracy of absolute data, an additional correction is necessary because of the deviation of the emissivity of water from 1.0 and the resulting reflection of atmospheric radiation.

Assuming emissivity data from Bramson (1964), Table 1, and estimating the effect from Kunde's 1965 graphs, a depression of equivalent

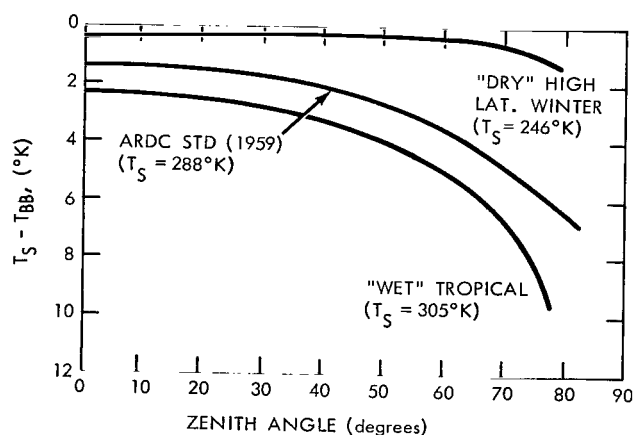


Figure 6—Theoretical surface temperature minus HRIR equivalent black body temperature difference as a function of zenith angle for three model atmospheres. A grey body surface emissivity of unity and clear sky conditions have been assumed (after Kunde, 1965).

black body temperature from true surface temperature by 0.7°K results, on the average, for zenith angles less than 60 degrees. The combined atmospheric and emissivity effect, which amounts to 2.7°K on the average ranges from +1°K (vertical view through a dry, high-latitude winter atmosphere) to 6.4°K (viewing at a 60-degree zenith angle through a very moist tropical atmosphere).

In summarizing, the theoretically derived total correction adds up to $+3.8 \pm 2.0^\circ\text{K}$, average. The single components are listed in Table 2. This is in good agreement with earlier experimental results from high-flying aircraft, as reported by Goldberg et al. (1964).

Instrument Noise

From the original analog records of two single scans of the spacecraft housing chosen at random during the period of the experiment, an average systems noise was determined to be $\pm 4^\circ\text{K}$. Contained in this noise are two components of particular interest—a permanent oscillatory component and a sporadic interference of reflected sunlight.

Although heavily reduced in amplitude when compared with Nimbus I HRIR measurements (Fujita and Bandeen, 1965), a residual oscillatory noise occurred in the Nimbus II HRIR measurements, as described by McMillin (1969). The noise frequency was found to be 200 Hz; the amplitude was about 2°K. Because of strong interference of this noise with the high-resolution temperature patterns required for oceanographic or geological applications of HRIR data, a mathematical filter was produced by McMillin to eliminate this noise component before map production from Nimbus meteorological radiation tapes.

This system noise is not reduced significantly by the routine averaging involved in the production of a large-scale grid print map; for example, in a 1:1 million map, only one to five individual scan spots are averaged per grid square. Thus the numerical filter must be applied. The effect of the filter is shown in Figure 8. However, if the number of points in the average approaches 15 or 20, as for example in a 1:3 million map, the spatial average itself becomes an adequate filter for most uses.

Besides the permanently present oscillatory noise, a second, sporadic noise component existed whenever the sun was close to the horizon. Direct sunlight was kept away from the sensor

Table 1

Emissivity of Liquid Water as a Function of Zenith Angle and Wavelength in the 3- to 4-Micron Window (after Bramson, 1964).

Wavelength, λ (μ)	Emissivity			
	$\theta = 0^\circ$	$\theta = 30^\circ$	$\theta = 60^\circ$	$\theta = 80^\circ$
3.40	0.966	0.965	0.919	0.622
3.50	0.969	0.968	0.924	0.627
3.60	0.972	0.971	0.928	0.632
3.70	0.974	0.973	0.931	0.638
3.80	0.976	0.975	0.935	0.643
3.90	0.977	0.976	0.937	0.646
4.03	0.978	0.977	0.938	0.648
4.10	0.978	0.977	0.938	0.648

Table 2

Theoretically Derived Average Corrections to Nimbus II HRIR Measurements of Equivalent Black Body Temperatures for Derivation of Sea Surface Temperature Under Clear-Sky Conditions.

Cause of Correction	Temperature (°K)
Microsurface effect	+0.6
Minor constituent absorption	+0.5
Water vapor and CO ₂ absorption	+2.0
Emissivity effect	+0.7

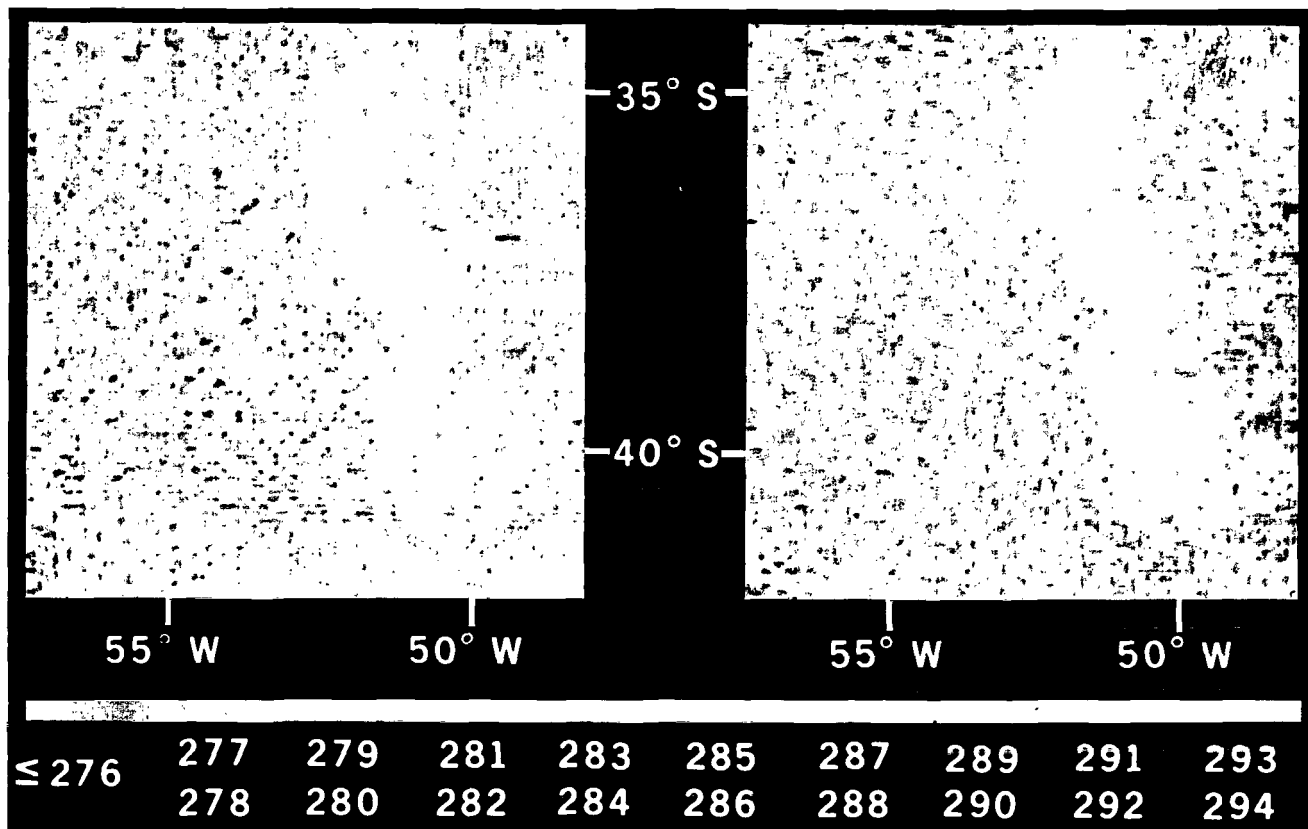


Figure 8—HRIR temperature patterns (in °K) derived from Nimbus II measurements on August 17, 1966 over the South Atlantic Ocean. The left one of the hand-colored figures shows raw data, the right one filtered data where the oscillatory noise has been removed. Notice the 'cleaner' pattern in the filtered version which also exhibits a number of more organized small-scale patterns than the unfiltered version.

by sunshields, but, as the measurements show, a small amount of sunlight scattered at parts of the spacecraft must have entered the radiometer near satellite sunrise and sunset. This scattered sunlight increased noise as well as the radiometer output, i.e., in measured equivalent black body temperature. The temperature increased approximately 6°K, average, as can be seen from Figure 9, in which the oscillatory noise was not eliminated. The scattered sunlight effect is visible in the upper portion of Figure 9, where the overall temperature increase of 6°K is clearly shown. In photofacsimile displays (Figure 10), the effect is noticeable because of a number of parallel, darker stripes across the affected portion of the picture.

Thus, in the areas of satellite day-night transition, which actually represent two very small sections of each orbit, an additional correction must be applied in order to derive accurate quantitative results.

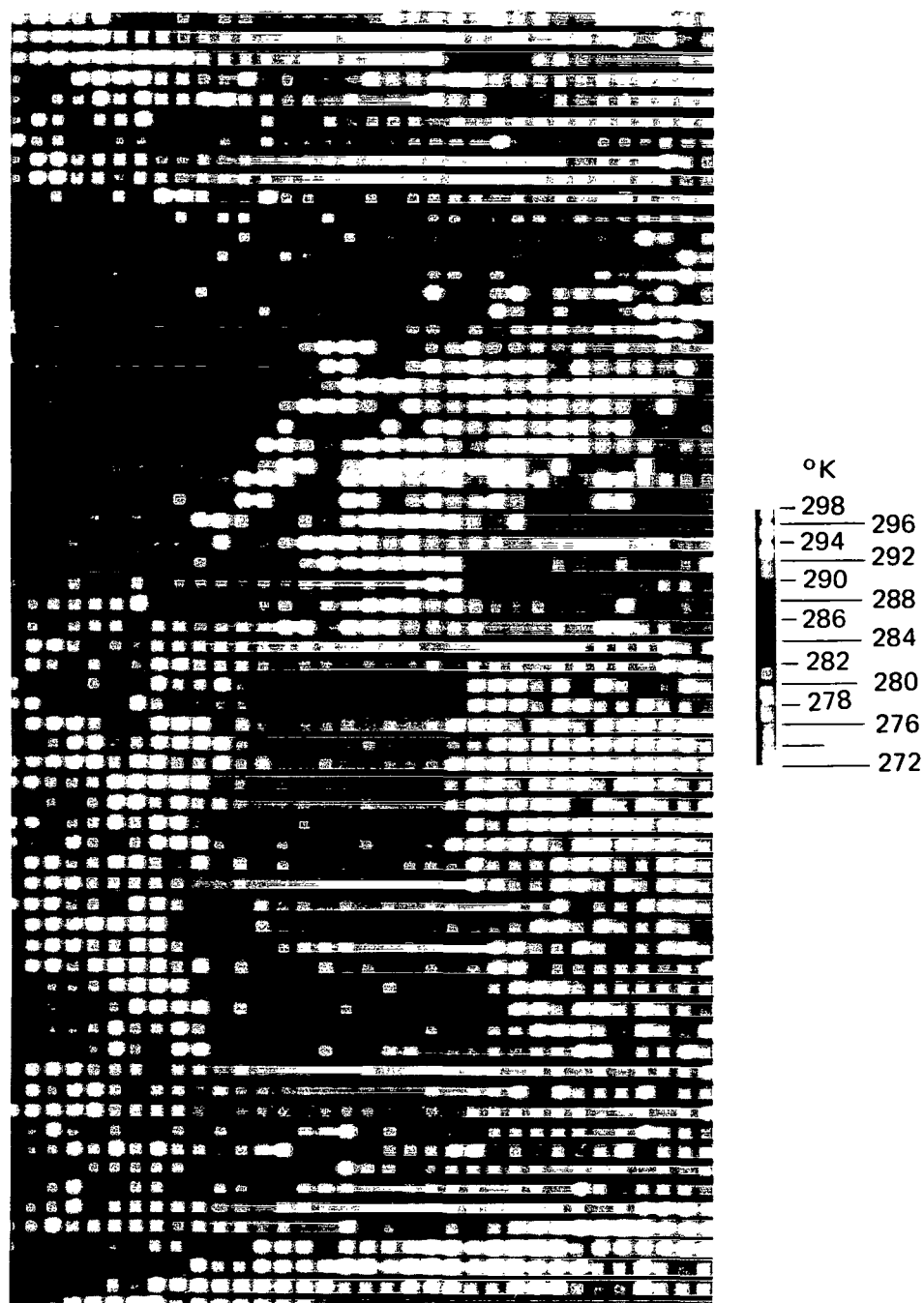


Figure 9—Digital color print of computer grid print map of Nimbus II HRIR measurements from orbit 1197 on August 13, 1966 over the Lake Michigan area. The zone of reflected sunlight interference during the satellite day-night transition is accentuated by the color selection. The predominantly red (land) and green (Lake Michigan) areas in the lower part of the picture are without interference. The predominantly blue (land) and Yellow-green (Lake Michigan and Lake Superior) areas to the north represent the affected region.

Data Location

In general, the grids that are automatically superimposed on the filmstrips are claimed to be accurate within 2 degrees of great circle arc at the subsatellite point. However, the grid location of the Nimbus II data was usually better, with errors exceeding 1 degree being rare. However, even an error of 1 degree at the subsatellite point causes a large error in the distorted region at the side of the filmstrips.

Contrary to the filmstrip grid, which used predicted orbital parameters to provide an approximate, real-time rectification of the analog data, actual orbital parameters were used to produce the Nimbus meteorological radiation tapes (NMRT). Hence, the data location in the grid print maps produced from the NMRT is claimed to be accurate within 0.5 degree of great circle arc. Although this was generally found to be true, a small uncertainty remains because no corrections were applied for pitch and yaw; however, these were proven to be small. Roll errors were eliminated automatically by the nature of the data location procedure within each individual scan. During the digitization process, the center of the swath was determined from the occurrence of the horizon on either side; the center was then located at the subsatellite point (nadir). Some small residual uncertainty can still occur, however, because of uncertainties in the definition of the actual horizon. This results in a location error of ± 0.5 grid intervals in a 1:1 million map (1 grid interval corresponds to $1/8$ degree longitude, i.e., 10 kilometers at 45 degrees latitude), as illustrated by Figure 11. In this grid print map showing equivalent black body temperatures around Lake Michigan close to local midnight on July 31, 1966, the contouring was chosen to accentuate the isotherm nearest the lakeshore. Because the eastern and western shore lines of Lake Michigan are fairly smooth and parallel, the small location error of the individual scan lines becomes recognizable. The data population in the map is 2 to 3 measurements, average, per grid point. Thus the general grid error of the entire map appears to be less than 0.2 degree of a great circle arc.

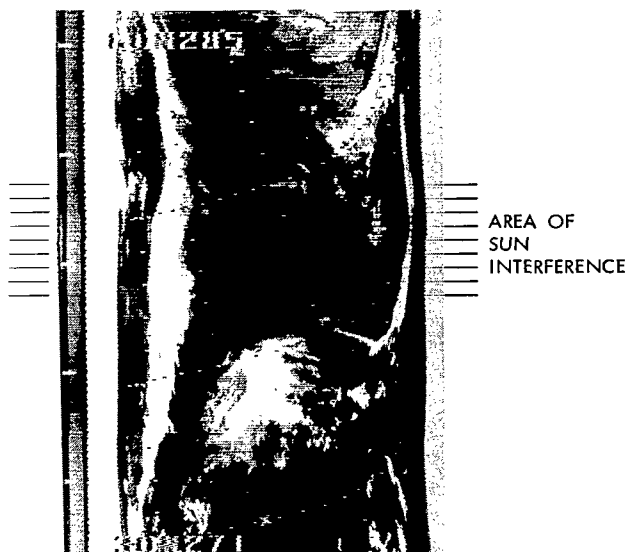


Figure 10—Photofacsimile print of Nimbus II HRIR data taken on August 13, 1966 on orbit 1197 showing, as indicated, the area of reflected sunlight interference during satellite day-night transition, recognizable by a broad band of darker stripes across the filmstrip.

SEA SURFACE TEMPERATURE PATTERNS DERIVED FROM NIMBUS II OBSERVATIONS

A systematic search for sea surface temperature features in the Nimbus II HRIR data was performed for the most spectacular surface temperature discontinuity, the north wall of the Gulf Stream off the United States east coast. Nimbus II HRIR photofacsimile data for the 174 days of HRIR operation revealed at least parts of the Gulf Stream boundary in 48 nighttime and 9 daylight cases. It should be mentioned that the daytime number is not representative because daylight data were obtained only for selected days. Some of the 57 cases will be presented and discussed in

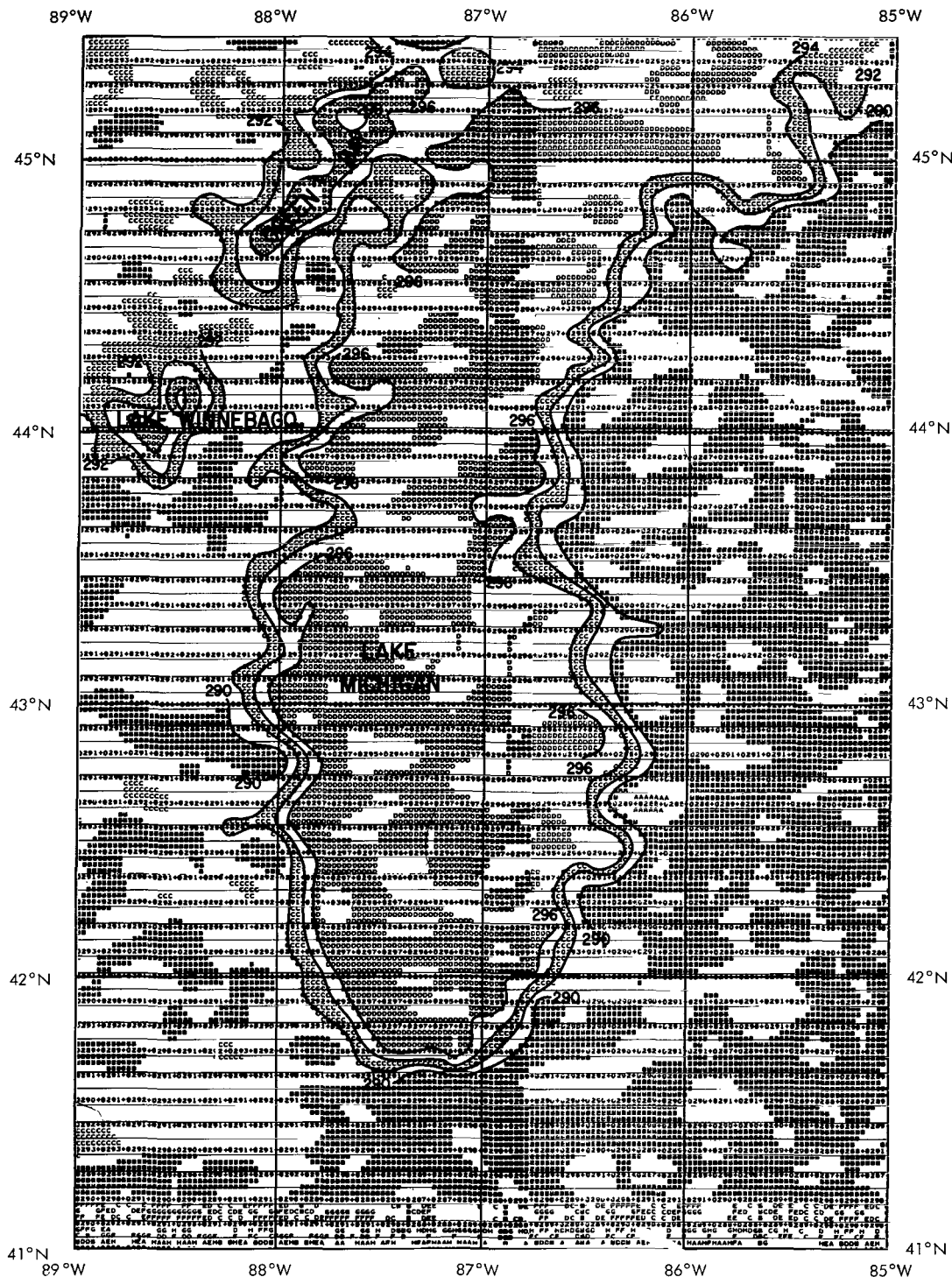


Figure 11—Section of the computer grid print map of Nimbus II HRIR nighttime measurements taken on July 31, 1966 (orbit 1024) over the Lake Michigan area. There are eight grid intervals per degree longitude. The superimposed grid represents the geographic grid produced by the computer for data location. Its accuracy is better than 0.2 degree of great circle arc. The outlines of the lakeshore are reflected by a sharp gradient in the printed equivalent blackbody temperatures (°K) as indicated by the drawn isotherms. The slight oscillation of these isolines is caused by small location errors of the individual scan lines.

Table 3

Indications of at Least Parts of the Gulf Stream Boundary from Nimbus II HRIR Measurements.

Datr (1966)	Data Orbit	Remarks	Date (1966)	Data Orbit	Remarks
May 30	198	Fair	October 1	1849	Good
June 2	238	Good	October 7	1929	Good
June 3	251	Good	October 8	1492	Excellent
June 4	265	Fair	October 9	1955	Poor
June 6	291	Fair	October 12	1995	Excellent
June 7	305	Fair	October 13	2009	Fair
June 15	411	Good	October 14	2022	Good
June 19	463	Fair	October 15	2035	Fair
June 22	504	Fair	October 16	2048	Fair
June 28	584	Fair	October 22	2128	Fair
July 1	634	Fair	October 28	2208	Fair
July 4	664	Excellent	October 29	2221	Fair
July 17	837	Poor	October 29	2222	Fair
July 22	904	Poor	October 30	2235	Fair
July 23	917	Good	October 31	2248	Poor
August 1	1037	Good	November 5	2315	Excellent
August 2	1050	Good	November 8	2355	Poor
August 12	1183	Good	November 10	2381	Poor
August 19	1276	Fair	November 15	2448	Fair
August 28	1396	Good			
August 30	1423	Fair	May 18	44	Fair, daylight
September 3	1476	Fair	May 18	45	Good, daylight
September 12	1596	Fair	May 20	71	Good, daylight
September 13	1609	Poor	May 23	111	Good, daylight
September 23	1742	Poor	May 24	124	Good, daylight
September 24	1756	Excellent	May 25	138	Fair, daylight
September 27	1796	Fair	June 22	510	Good, daylight
September 27	1795	Fair	June 22	511	Good, daylight
September 30	1836	Fair	June 24	537	Excellent, daylight

this report; a complete listing of available Gulf Stream cases is given in Table 3. The remarks refer to how well the Gulf Stream boundary can be distinguished in the HRIR data.

Daytime Infrared Observations

Nine daylight cases indicating sea surface temperature characteristics in the Gulf Stream area are contained in the Nimbus II HRIR data volume (Nimbus Project, 1967). One of these and two other cases of indications of the Brazil and Falkland Currents boundary were selected for illustration in this paper.

The Brazil and Falkland Current Boundary

Photofacsimile pictures of the HRIR measurements and television photographs (AVCS) taken near local noon on May 25, 1966 by Nimbus II are reproduced in Figures 12 and 13. In the HRIR picture, the light-to-darker grey tones indicate low-to-higher radiances. The combined temperature

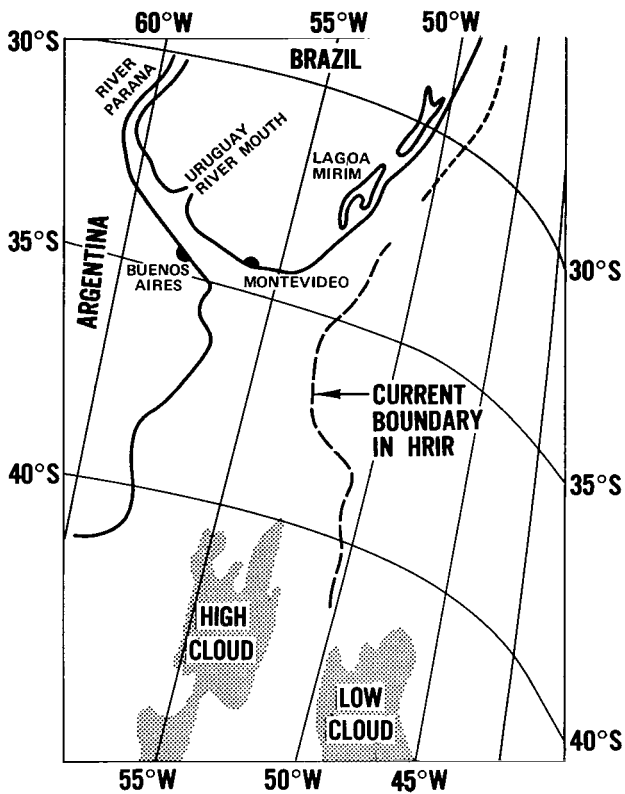
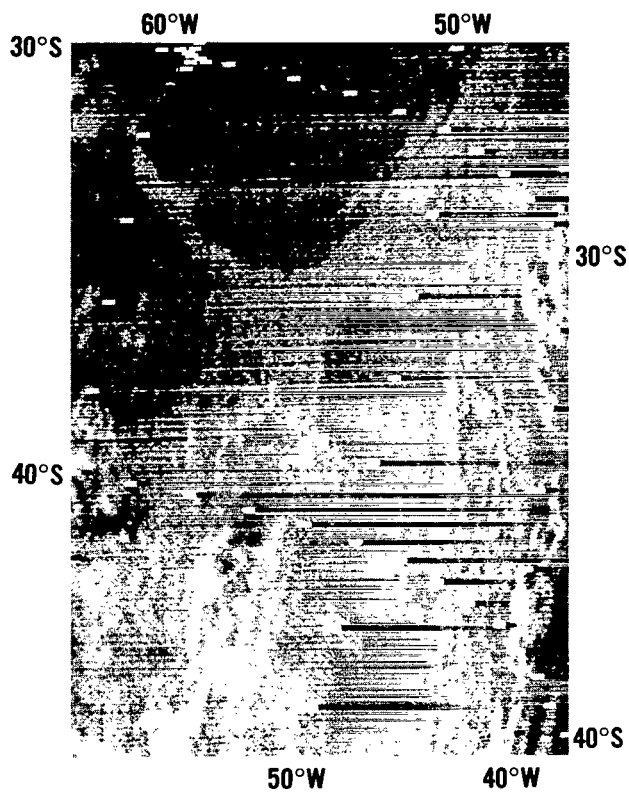


Figure 12—Photofacsimile and schematic analysis of Nimbus II HRIR daytime measurements taken on May 25, 1966, 1546 GMT (orbit 137), over the South Atlantic Ocean.

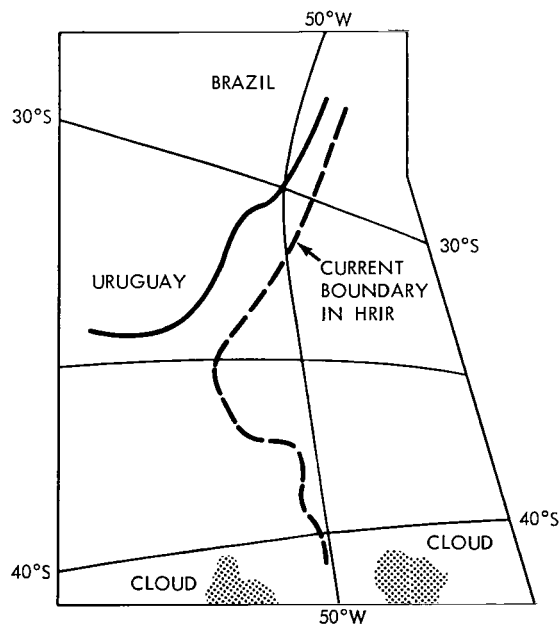
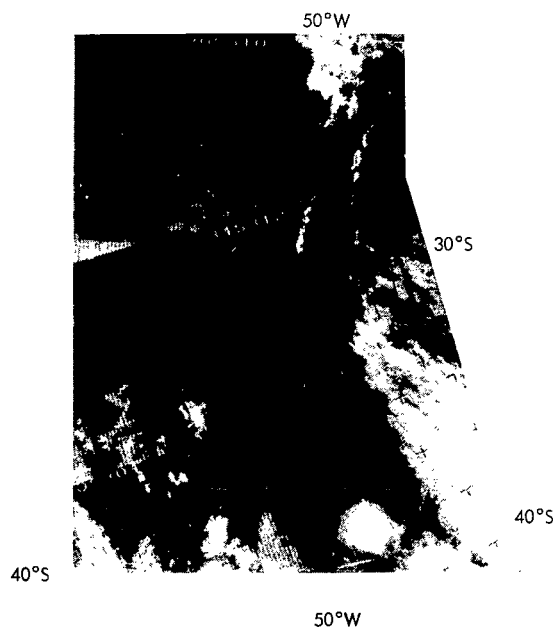


Figure 13—Mosaic and schematic analysis of Nimbus II AVCS television photographs taken on May 25, 1966, 1546 GMT (orbit 137), over the South Atlantic Ocean.

and albedo contrast between land and water is clearly pronounced in the images of outgoing radiance, revealing fine details such as the Rio de La Plata, the Parana River system, the mouth of the Uruguay River, and the large lagoons near the coast of Southern Brazil. An interesting detail that was visible in the original photograph is that large cities such as Montevideo and Buenos Aires were indicated as dark spots of higher radiance because of higher surface temperature and higher reflectivity. Over the ocean, a sharp discontinuity in radiance was found along the boundary between the southward-flowing, warm Brazil Current east of 50° to 53°W and the colder Falkland Current heading north closer to the South American coast (Figure 12). A mosaic of the concurrent cloud photographs is given in Figure 13. By comparing simultaneous television and infrared observations, cloudfree areas can definitely be depicted. Large parts of the discontinuity in the HRIR measurements were located under clear skies and therefore can be interpreted as sea surface temperature discontinuity although quantitative temperature values cannot be derived for reasons explained previously. The HRIR data in Figure 12 show that clouds can appear darker or lighter than surface features, depending on their actual temperature. The large cloud system consisting of two major cloud masses that extend southward from 40°S , 50°W on both sides of 50°W has the eastern cloud mass darker than the western, indicating that the eastern clouds are at a lower level. However, in the television pictures, Figure 13, both of these cloud masses appear almost equally bright. It is also seen in the HRIR data that the eastern cloud mass is also darker (meaning warmer) than the cold Falkland Current farther to the north.

A phenomenon of particular interest in this case is the distinct cloud band about 100 km to 200 km off the Brazilian coast between 26°S and almost 33°S . This pronounced line of clouds is very near the temperature discontinuity (current boundary) in the HRIR measurements and seems to indicate, in the way described during the discussion of cloud photographs taken over the Humboldt Current, the upward branch of the local vertical motion system induced by differential heating along the line of sea surface temperature contrast. It should be considered, however, that the upward motion most likely occurs several kilometers inside the area of warmer water rather than at the discontinuity itself. This example demonstrates the advantage of simultaneous multispectral observations in complementing each other and thus favoring a more valid and useful interpretation of each of the observations.

The second selected case shows the Falkland and Brazil Current boundary 1 month later, near local noon on June 24, 1966. In this case, the current boundary is not delineated by a cloud line and appears, for longer distances, under clear skies which favors the interpretation of the daytime HRIR observations (Figure 14). A discontinuity in radiance (grey tone) can be followed along a nearly meridional line across the entire picture, as indicated in Figure 14. Comparing this line with the cloud photograph in Figure 15 shows that the section between 32° and 39°S of this discontinuity is in clear air and therefore must represent a sea surface temperature feature. Farther south, this conclusion is no longer certain because the discontinuity follows the boundary of an extended cloud system too closely. It is likely, although not conclusive, that this apparently low-level, convective cloud system is caused by slightly decreased vertical stability over the warmer water surface in an air mass of nearly adiabatic lapse rate. Such a case is theoretically plausible, and a very pronounced real case has been reported by Warnecke et al., 1968. However, no

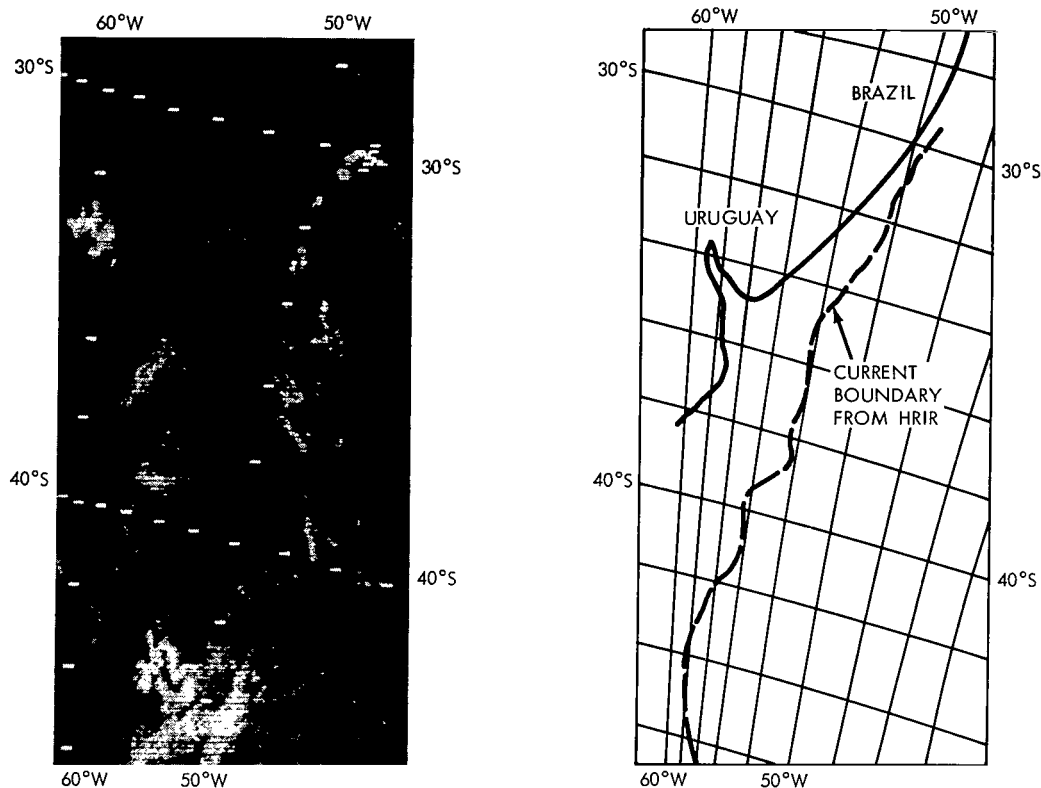


Figure 14—Photofacsimile and schematic analysis of Nimbus II HRIR daytime measurements taken on June 24, 1966, 1500 GMT (orbit 536), over the South Atlantic Ocean.

substantiating evidence can be brought in this case; therefore the current boundary indicated in Figures 14 and 15 must be considered uncertain south of the bar marked near 39°S.

The Gulf Stream

The third example of daytime HRIR data was taken over the Gulf Stream area also on June 24, 1966. A photofacsimile of these measurements is shown in Figure 16. Again, the land and water contrast caused by the temperature and reflectivity contrast under clear-sky conditions is very obvious in the observed radiances. Geographic outlines of the United States east coast can be recognized easily (Figure 16). Over the ocean, the pronounced discontinuity extending northeastward from about 70 km off Cape Hatteras can be interpreted in most portions as the sea surface temperature discontinuity along the north wall of the Gulf Stream. Patches of cirrus, which are white in Figure 16 because of their low temperature and are easily identified by their structure and thin appearance in Figure 17, are located in only a few minor areas near or over the boundary to the extent that they mask its location. Toward the southwest, along the Carolina coast, the current boundary is not defined as sharply but can still be traced. The southeastern boundary of the Gulf Stream is naturally a much less defined feature in the HRIR picture, but at least indications can be seen of this boundary zone which seems to follow parallel to the meandering north wall.

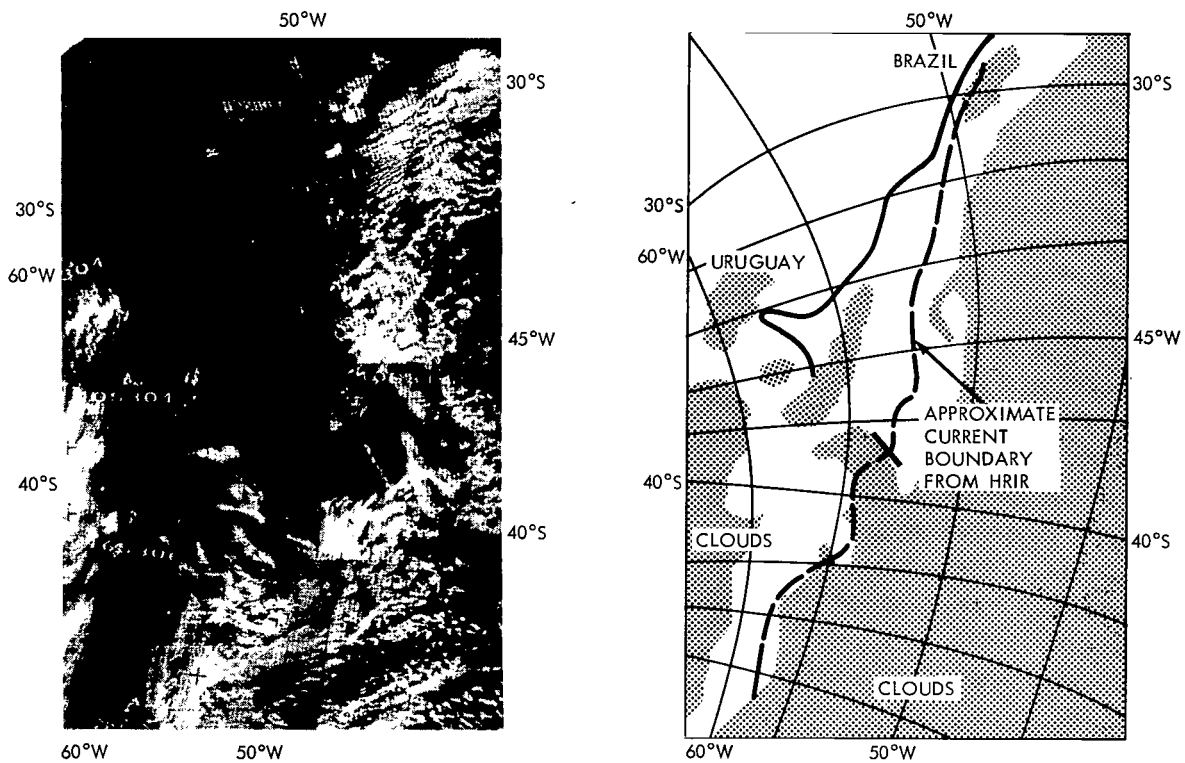


Figure 15—Mosaic and schematic analysis of Nimbus II AVCS television photographs taken on June 24, 1966, 1500 GMT (orbit 536), over the South Atlantic Ocean.

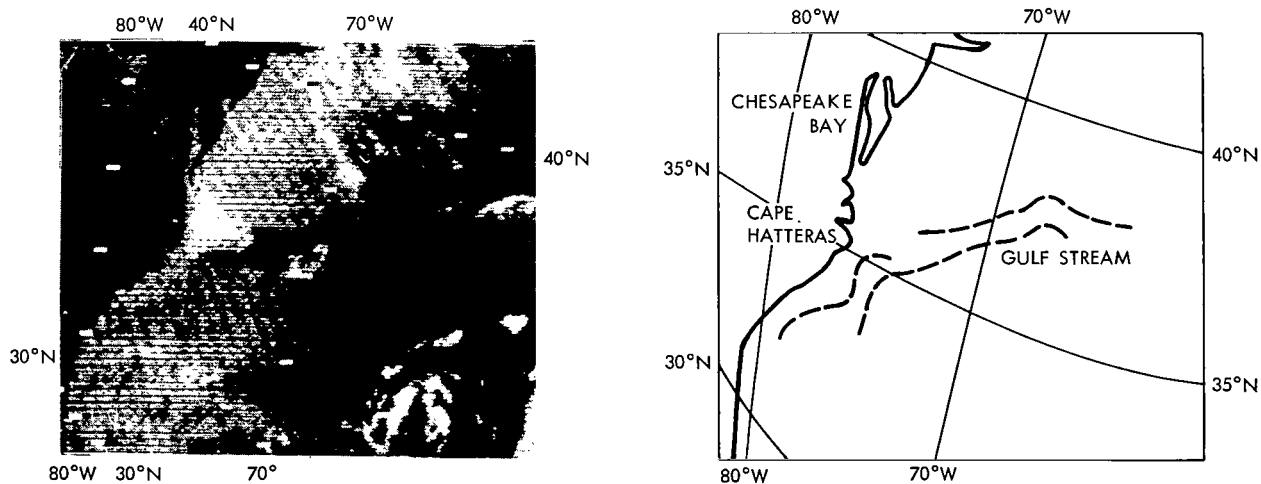


Figure 16—Photofacsimile and schematic analysis of Nimbus II HRIR daytime measurements taken on June 24, 1966, 1528 GMT (orbit 538), over the North Atlantic Ocean.

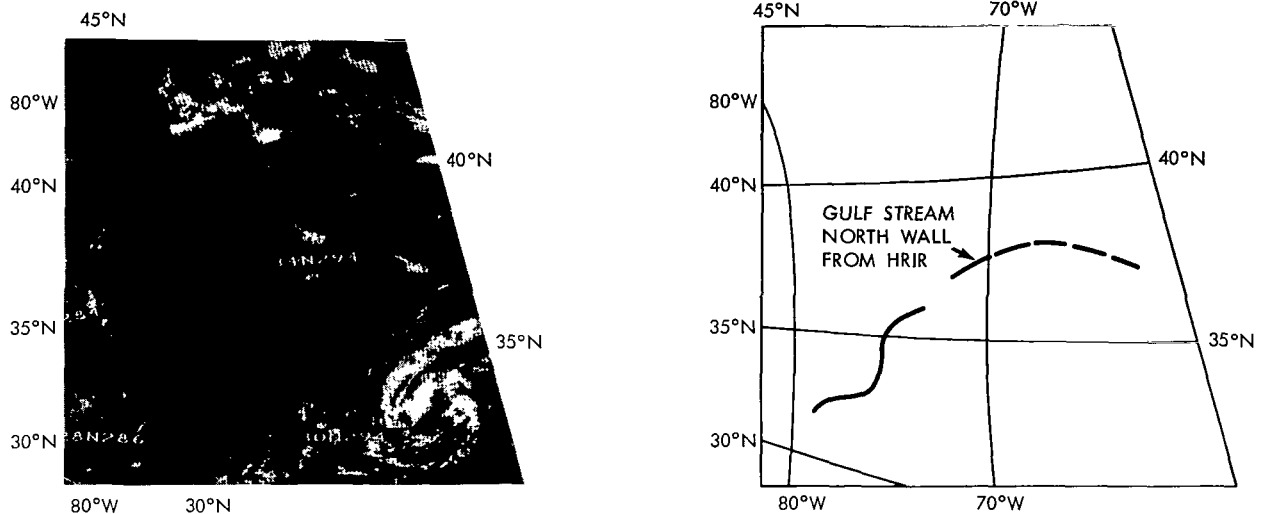


Figure 17—Mosaic and schematic analysis of Nimbus II AVCS television photographs taken on June 2, 1966 1528 GMT (orbit 538), over the North Atlantic Ocean.

These three cases show that infrared measurements in the 3- to 4-micron window allow the observation of oceanographic features under daylight conditions from a satellite. In conjunction with simultaneous cloud photography, it is possible to outline the location of sharp sea surface temperature contrasts such as those existing along the north wall of the Gulf Stream and along the divide between the Brazil and Falkland Currents.

Nighttime Infrared Observations

Definition of the Gulf Stream Boundary

The inshore boundary of the Gulf Stream was defined by Fuglister and Worthington (1951) as the line of no horizontal pressure gradient. Generally, the horizontal temperature discontinuity at 200-meter depth is considered as the actual current boundary location. The boundary surface, however, is inclined by approximately $1/3$ to $1/2$ degree from the horizontal plane. Thus, at the immediate sea surface, the boundary appears approximately 25 to 40 km north of the actual stream boundary (Stommel et. al., 1953, Stommel, 1965). This surface temperature discontinuity was observed by the remote sensing techniques and will be discussed here.

The Gulf Stream North Wall

Nighttime HRIR sea surface temperatures recorded over the northern edge of the Gulf Stream on June 2, 1966 are presented in Figure 18. This black-and-white filmstrip is based on the original data received at the ground station and therefore contains the oscillatory noise described earlier. The first-hand analysis shown in Figure 19 is based on a digitized version of the same data and therefore contains this noise component also. Because of the smoothing process involved

in this isothermal analysis, part of the noise seems to be eliminated; however, other parts might have been emphasized by this subjective process. In spite of this fact, the main characteristics of the sea surface temperature pattern stand out clearly and demonstrate the capability of the method. Although cloud interference by a cold front was observed over the main body of the Gulf Stream and sporadically in other parts of the figure, the north wall of the ocean current was well pronounced over a distance of approximately 700 kilometers. It is characterized by a small zone of strong temperature-contrast of approximately 10°K , average, across a distance of 10 kilometers between 71° and 76°W , as indicated by the approximately parallel heavy lines in Figure 19. This zone appears as a sharp discontinuity in grey tone in the photograph (Figure 18). The actual temperature in these infrared data was about 300°K over the warmer Gulf Stream waters, which appear darker in the picture, and about 290°K over the cooler slope waters to the north, appearing lighter in the photograph.

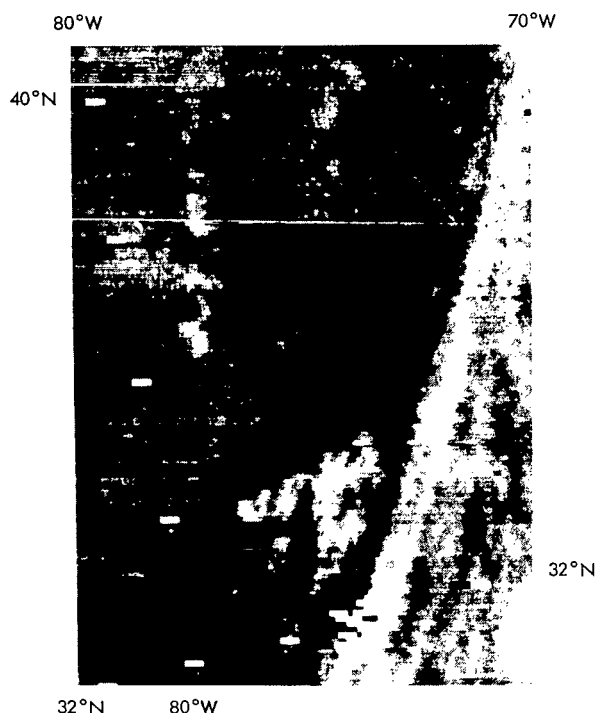


Figure 18—Photofacsimile of Nimbus II HRIR nighttime measurements on June 2, 1966, 0507 GMT (orbit 238), over the North Atlantic Ocean near the United States coast.

A reanalysis of this case after use of a filter program to eliminate the periodic noise is reproduced in Figure 20. Although details changed, the overall picture remained the same, and the Gulf Stream boundary stood out even more clearly than before. Figure 21 shows the same data in an improved form of data display—the computer grid-print map in a Mercator projection of eight grid points per degree longitude with the third dimension (temperature) transformed into a selected color scheme. Each color square corresponds to the temperature at one grid point; the temperatures are translated into distinct colors in 2°K intervals. The Gulf Stream boundary, accentuated by the specific color selection used, is visible along the northern edge of the red and purple areas (warmer than 296°K) where a sharp transition to green (286° to 292°K) can be observed. With regard to the absolute values of the measurements presented in this case, it is important to notice that from the northern margin southward to approximately Cape Hatteras interference by sunlight reflected from spacecraft parts, as described earlier, occurred; it is indicated by the pattern of broad, darker streaks across the upper part of Figure 18 and by the shift of red to purple and light green to dark green in the upper part of Figure 21.

The HRIR measurements on August 28, 1966 were selected as a second case of study. Although in this season the temperature contrast between the Gulf Stream and the slope water is significantly reduced, the inshore edge of the Gulf Stream is still pronounced in the photographic

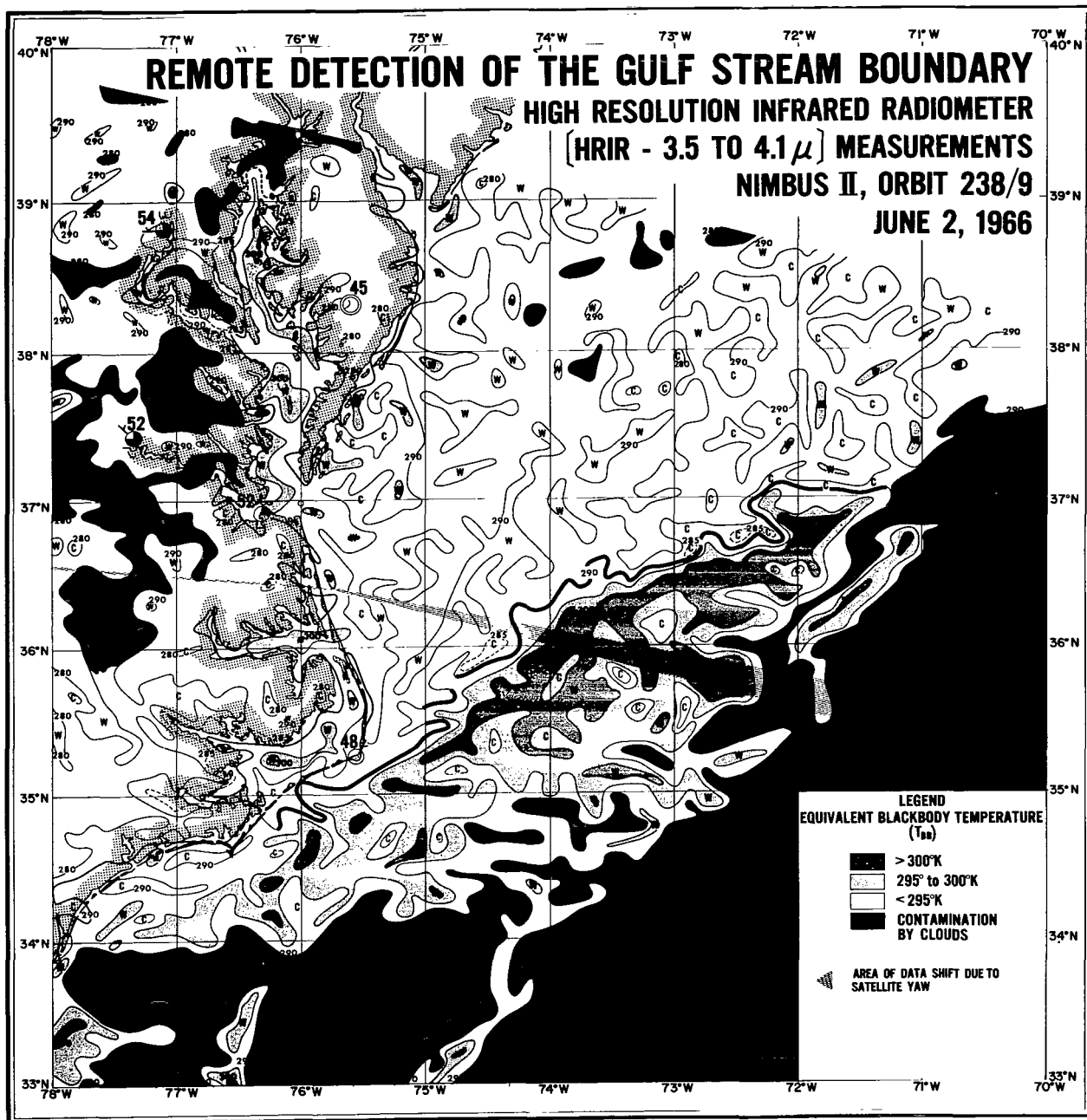


Figure 19—First analysis of Nimbus II HRIR nighttime measurements over the Gulf Stream taken on June 2, 1966 (Allison et al., 1967), based on the unfiltered data. Isotherms are drawn in 10°K intervals; additionally, the 295°K isoline is shown.

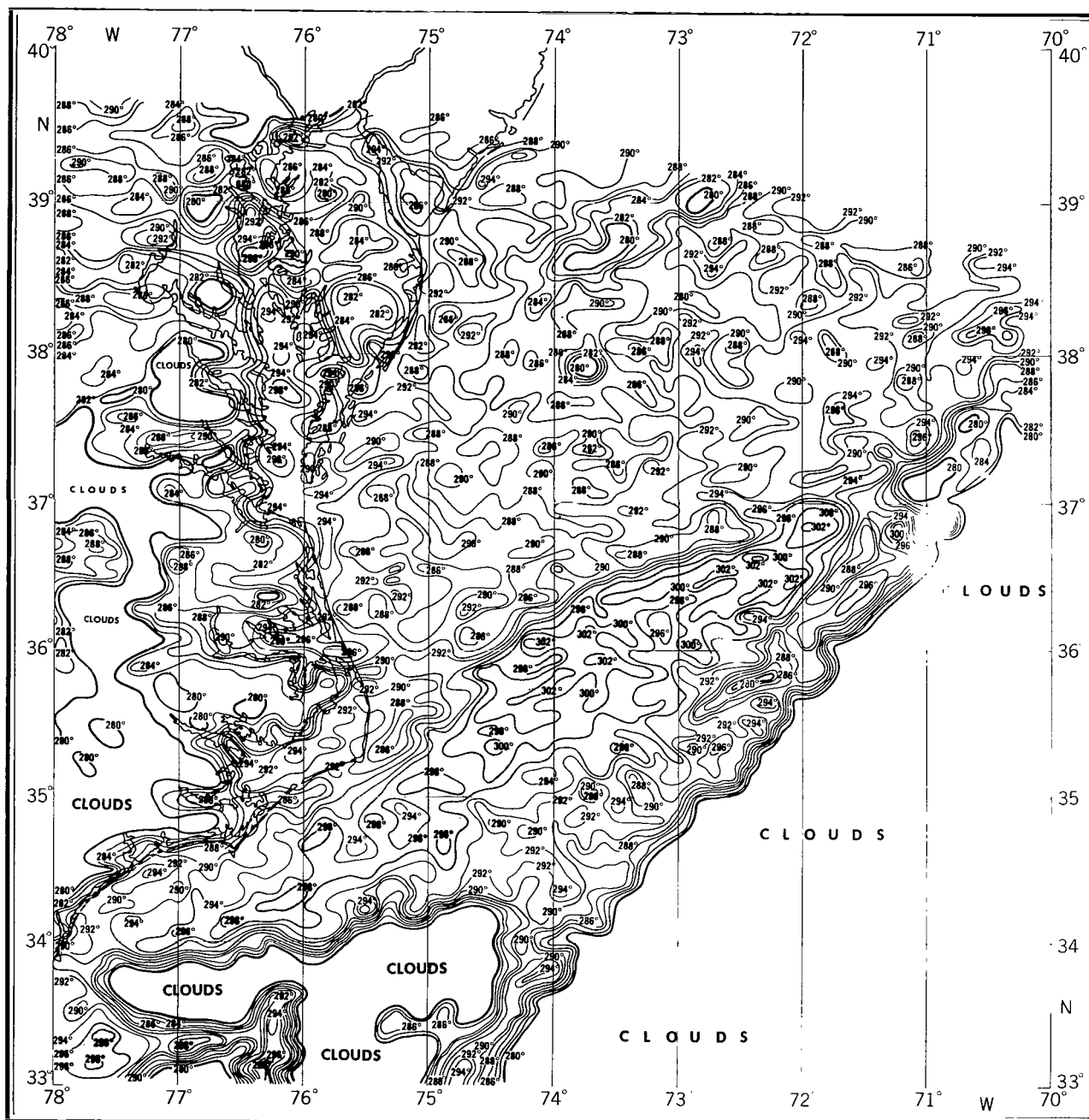


Figure 20—Reanalysis of Nimbus II HRIR nighttime measurements over the Gulf Stream taken on June 2, 1966 (orbit 238). Isotherms are drawn in 2°K intervals. The shaded area indicates those parts of the Gulf Stream seen by the radiometer without cloud contamination.

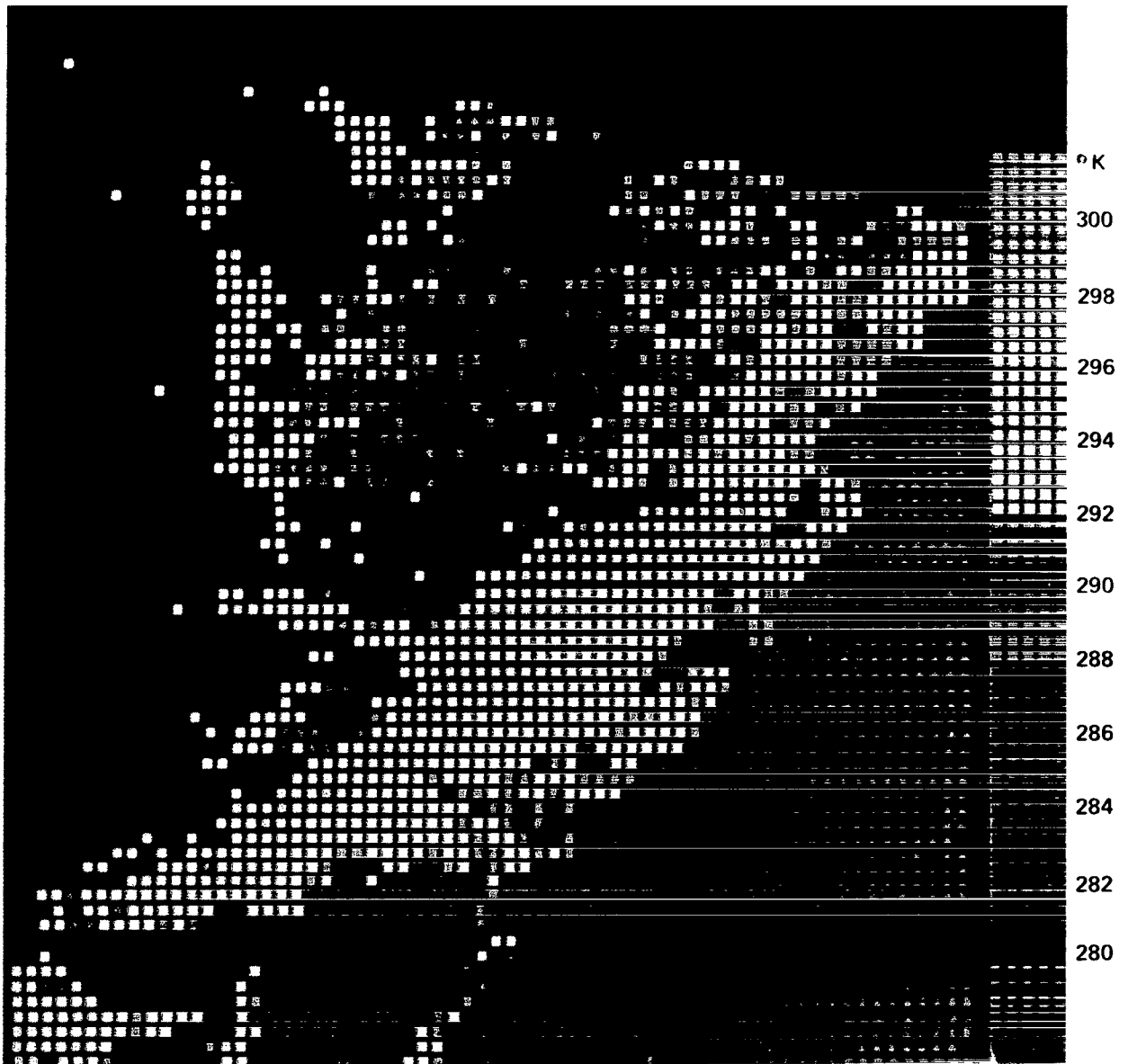


Figure 21—Digital color print of computer grid print map of Nimbus II HRIR measurements from orbit 238 on June 2, 1966 over the Gulf Stream (oscillatory noise eliminated by numerical filter). Blue and grey areas indicate clouds and/or land. The North Wall of the Gulf Stream stands out under clear skies; its southern boundary is obscured by clouds. Note the higher temperatures shown in Chesapeake Bay and the Delaware River if compared with the near-shore ocean temperatures.

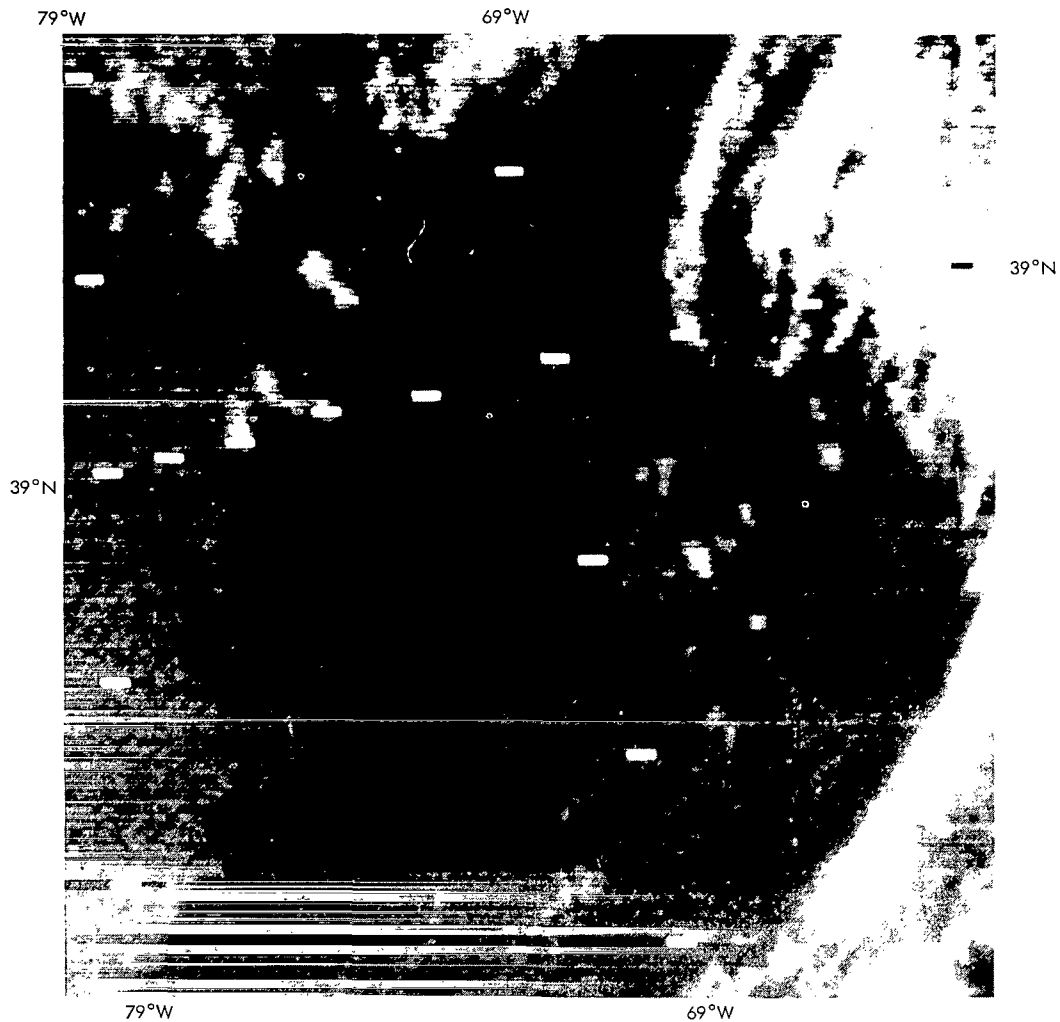


Figure 22—Photofacsimile of Nimbus II HRIR nighttime measurements taken on August 28, 1966, 0440 GMT (orbit 1396), over the Gulf Stream area. The denumeration of the geographic grid takes into account an obvious error in the automatic picture grid.

image (Figure 22) and in the colored version of the digital computer printout (Figure 23). The striking phenomenon of this case is the strong meander of the Gulf Stream between 67° and 73° W, which is in good agreement with the documented Gulf Stream positions for this month (U. S. Naval Oceanographic Office, 1966). The Gulf Stream temperatures are shown between 296° and 300° K on the average, with a few spots warmer than 300° K. The slope water temperature ranges mainly from 292° to 296° K. This example demonstrates that even in the season with minimum temperature contrast the HRIR method is capable of detecting the northern Gulf Stream boundary.

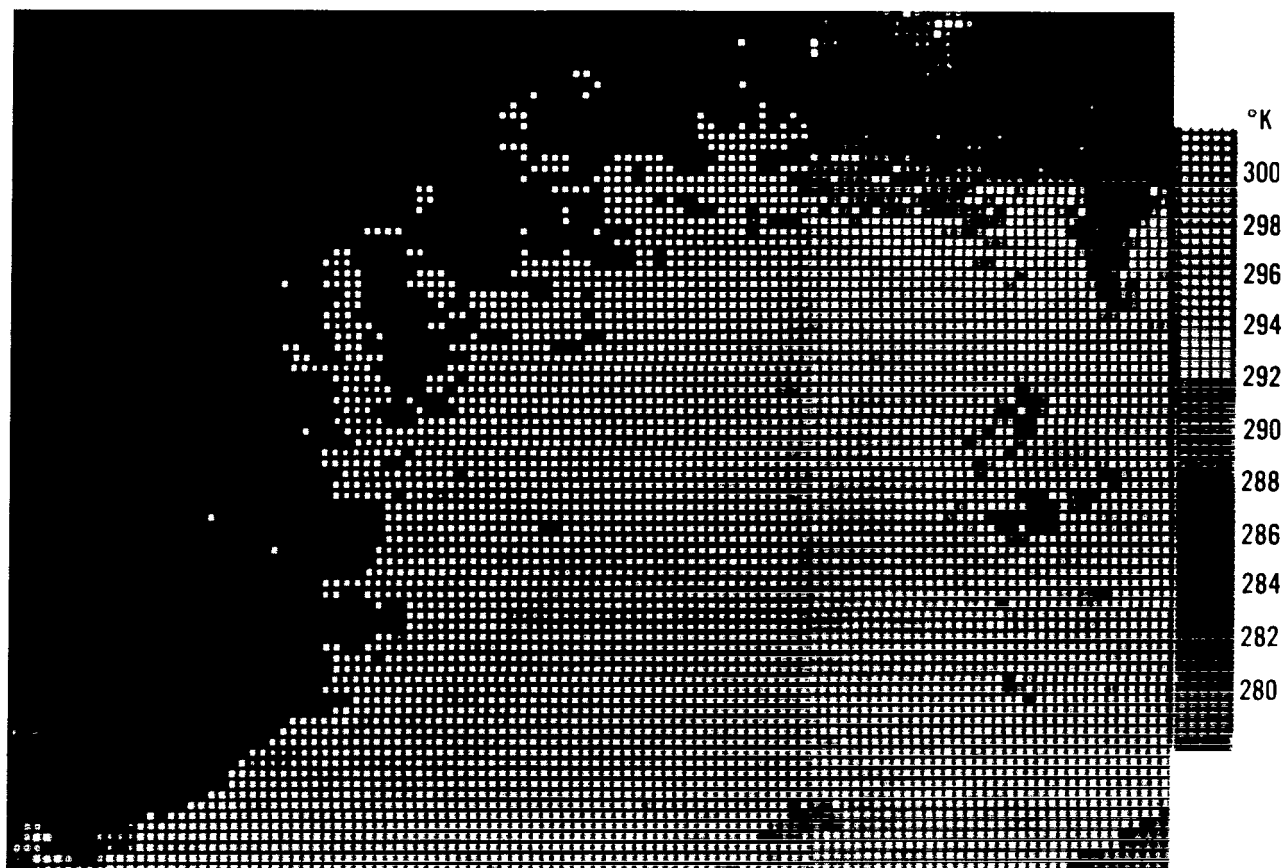


Figure 23—Digital color print of computer grid print map of Nimbus II HRIR measurements from orbit 1396 on August 28, 1966, 0440 GMT, over the Gulf Stream. The northern boundary of the Gulf Stream is indicated by the transition from darker red (more than 296°K) to orange and yellow (292° to 296°K). Green, blue, and grey represent clouds and land.

Comparison with Aircraft and Shipboard Measurements

In both of the preceding cases, simultaneous radiometric observations of the sea surface temperature structure from low-flying aircraft were available for comparison. The airplane, operated by the U. S. Naval Oceanographic Office, routinely maps the northern edge of the Gulf Stream between 65°W and 75°W. It is equipped with a Barnes infrared radiometer that is sensitive from 7.3 to 13.5 microns, has a 2.2-degree square, fixed field of view, and in flight is accurate to $\pm 0.4^{\circ}\text{K}$ 95 percent of the time. The airplane track is determined by Loran A. The navigational accuracy of Loran A over the Gulf Stream area is better than 4 km between 63°W and 75°N, according to the U. S. Naval Oceanographic Office (1967).

The airplane usually performs two tasks. It tracks the inshore surface boundary of the Gulf Stream and records continuously the sea surface temperature profile across the detected boundary and over the other ocean areas to and from the scene. During the tracking portion of the mission, the aircraft is steered back and forth across the zone of strong temperature gradient with the aid of an infrared radiometer indicator in the cockpit.

The results of the research flight on June 2, 1966 are shown in Figure 24. The flight, conducted at night, commenced just before and extended slightly beyond the actual time of the Nimbus II overpass. The heavy dots are positions where the strong temperature gradient was located, and the solid lines with tick marks and temperatures are the tracks along which temperature profiles were taken. The temperatures shown are average values between two tick marks. These airplane data were superimposed on the almost simultaneously taken Nimbus II HRIR data analyzed from a high resolution computer printout. It can be derived from this figure that the zone of sharp temperature gradient in the HRIR data coincides surprisingly well with the locations detected by the aircraft, particularly if one considers the uncertainties involved in the location of both of the data sets. The average distance between the 27 marked Gulf Stream boundary locations from aircraft detection (black dots) and the center of the zone of strongest horizontal gradient of sea surface

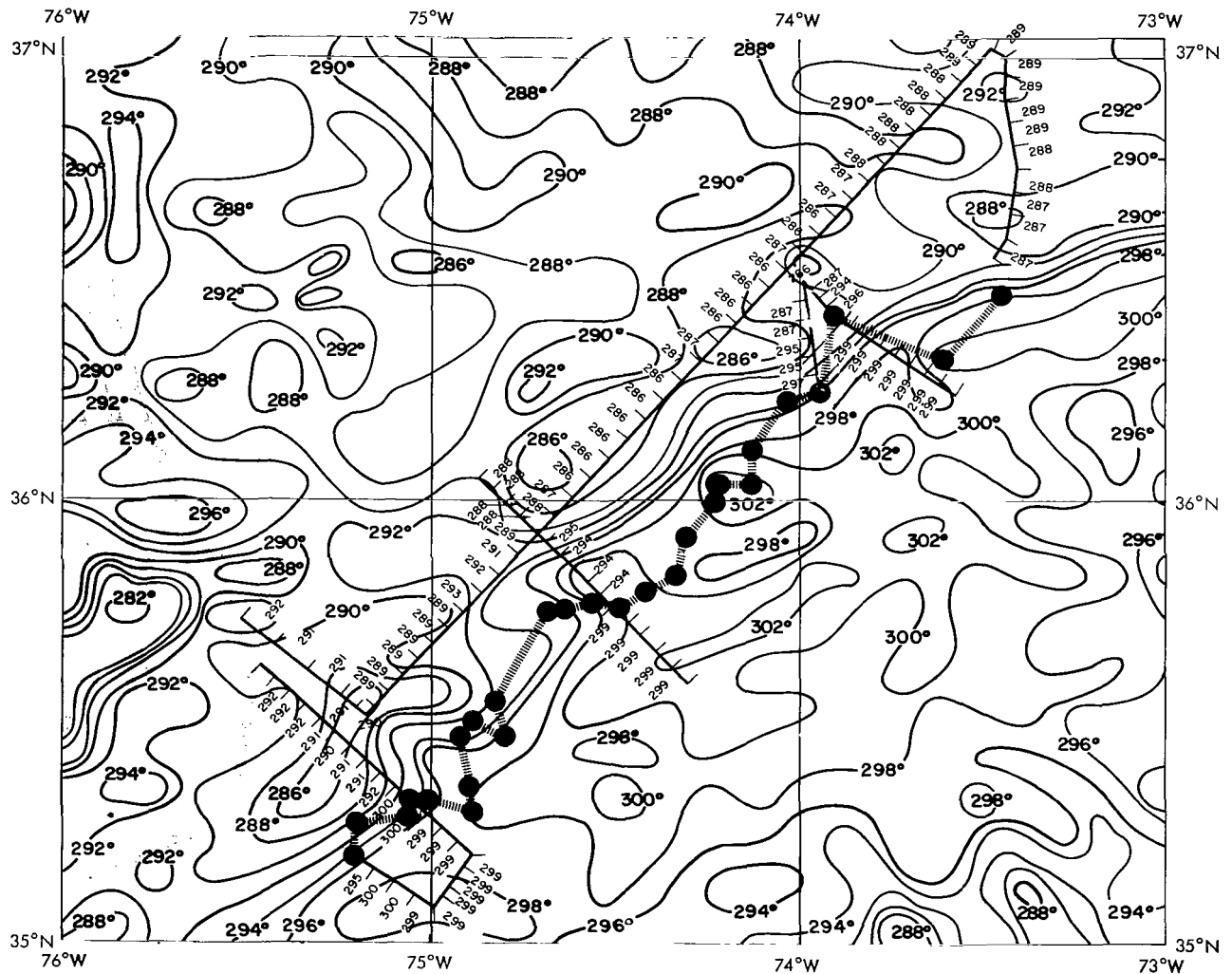


Figure 24—Comparison of simultaneous Nimbus II HRIR (orbit 238, 0500 GMT) and aircraft radiometric nighttime measurements (0300 to 0630 GMT) of sea surface temperature near the northern Gulf Stream boundary on June 2, 1966. Heavy dots represent the location of the Gulf Stream boundary as detected from the aircraft. Numbers along the tracks of specially flown horizontal temperature profiles represent average sea surface temperatures (in °K) between tick marks.

temperature detected from the satellite is 12 kilometers. For the temperature comparison, some data near the strongest gradient zone had to be excluded in order to diminish mere location errors. The average temperature difference between the aircraft and the satellite measurements for the remaining 94 pairs of simultaneous data was determined to be 0.45°K ; that is, the satellite data were, on the average, about 0.5 degree too warm. From the theoretical considerations previously discussed, the satellite data should give values that are too low by approximately 4°K (see Table 2). Because of interference caused by sunlight scattered from parts of the spacecraft, an error of $+6^{\circ}\text{K}$ must be assumed in this part of the orbit. Thus, both systematic errors appear largely to compensate each other, and sea surface temperature should be indicated 2°K too warm by the HRIR measurements. The observed difference of $+0.45^{\circ}\text{K}$ can well be considered reasonably small and within the limits of accuracy of this error analysis.

In the southern part of the Gulf Stream region of Figure 20, ship data were also available for comparison. Research vessel EASTWARD of the Research Triangle Institute, North Carolina, was cruising across the Gulf Stream between May 23 and 28, 1966. Its temperature measurements are plotted in Figure 25. With regards to the sea surface temperature distribution, these measurements are fairly representative for the day of the Nimbus II overpass, June 2, 1966. Unfortunately, most of the ship data were located in the area where the satellite data were disturbed by clouds. Thus, a direct comparison was possible in only a few locations. Nevertheless, the ship measurements verified that the Gulf Stream temperatures were 297° to 299°K , thus confirming the airplane and satellite measurements. The inner edge of the Gulf Stream was found near 34.6°N , 76°W by the EASTWARD, and the Nimbus II data, taken 10 days later, show the strongest horizontal temperature gradient in almost the same position.

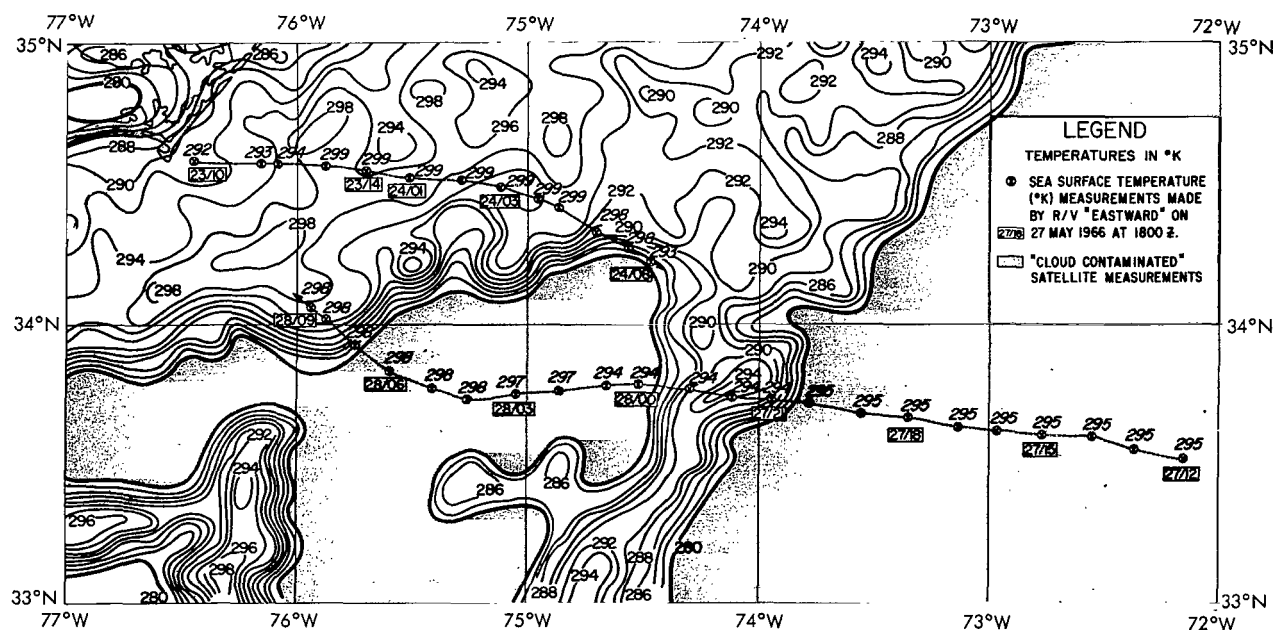


Figure 25—Comparison of Nimbus II HRIR nighttime measurements on June 2, 1966 (orbit 238) with temperature measurements from shipboard (R/V EASTWARD) between May 23 and 28, 1966.

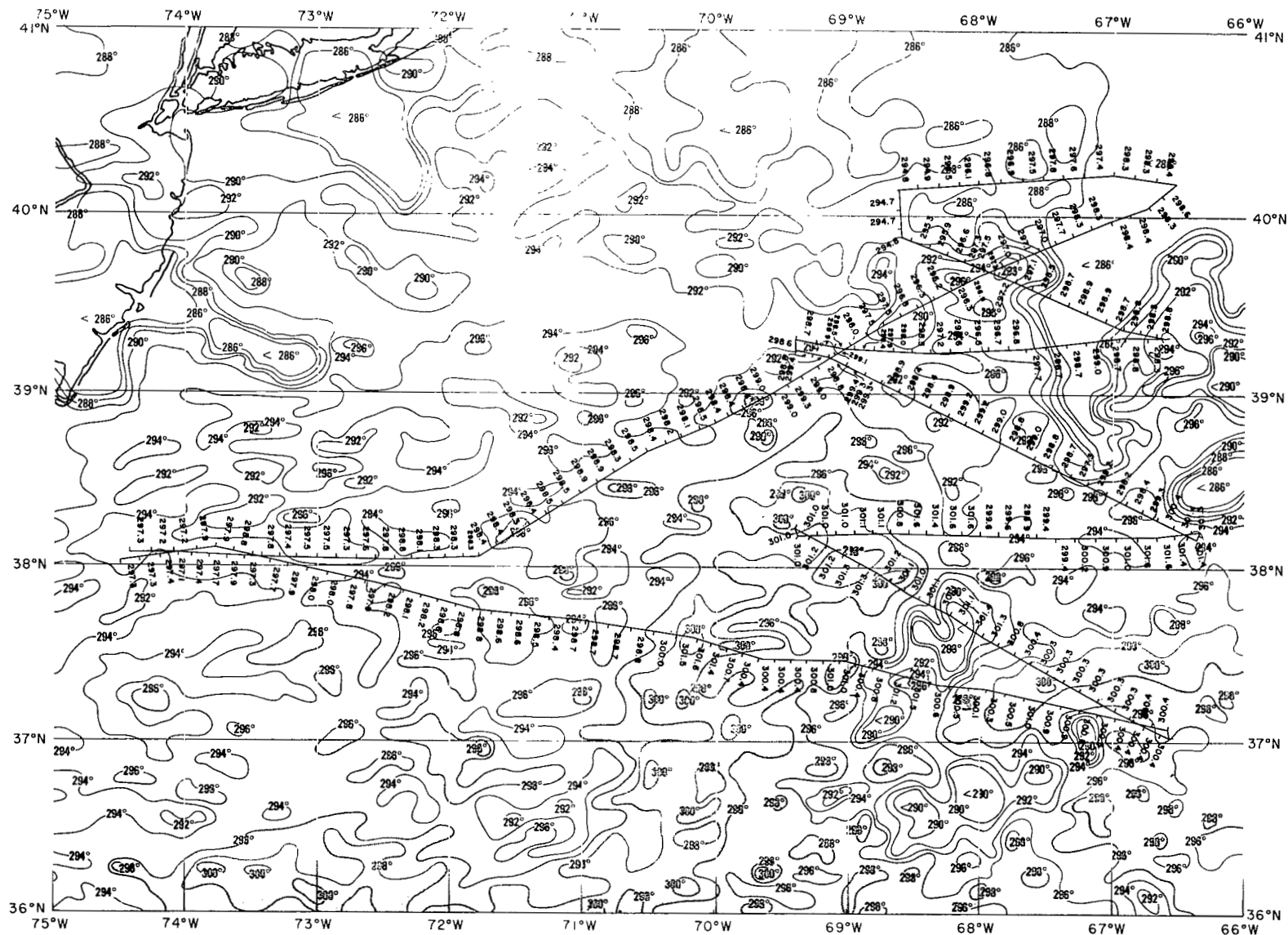


Figure 26—Comparison of Nimbus II HRIR nighttime measurements on August 28, 1966, 0440 GMT (orbit 1396), with radiometric aircraft measurements on August 27, 1966, 1200 - 2100 GMT. Numbers along airplane tracks are temperatures (in °K) averaged between tick marks.

On August 28, 1966, data from another research flight over the Gulf Stream were available for direct comparison with Nimbus II measurements. These flight data, unlike those of June 2, were taken during daylight hours approximately 6 to 18 hours after the Nimbus II overpass. In this case, no interference by scattered sunlight was observed in the satellite data. The airplane track and the results of the temperature measurements taken along these tracks are reproduced in Figure 26. A numerical evaluation for 196 pairs of simultaneous measurements without apparent cloud contamination of the satellite data revealed that the Nimbus II HRIR measurements were 3.9°K colder than the concurrent airplane data. This temperature difference is within 0.1°K of the theoretically expected value. However, the theoretical considerations were based on standard atmosphere conditions, and it is reasonable to assume that in different seasons and locations, larger differences between theoretical and observed data may occur unless more realistic atmospheres are used for the theoretical computations. Ideally, corrections were to be computed from simultaneously taken spectrometric measurements of the actual vertical water vapor profile as suggested by the Nimbus III IRIS (Infrared Interferometer Spectrometer experiment).

The Brazil and Falkland Current Boundary

In addition to the daylight cases presented earlier, two cases of nighttime observations—only 24 hours apart—of the boundary between the warm Brazil and the cooler Falkland Current were selected from the Nimbus II HRIR data for presentation. On August 16, 1966 behind northeastward-

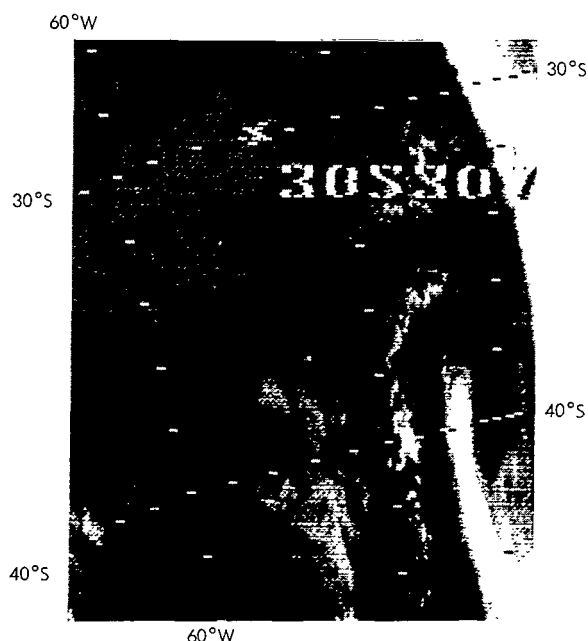


Figure 27—Photofacsimile of Nimbus II HRIR nighttime measurements on August 16, 1966, 0245 GMT (orbit 1235), over the Atlantic coast of South America.

moving cold front, large parts of this boundary were under clear skies. Besides other very prominent features such as the South American coast, the La Plata River mouth, and details such as the Parana and Uruguay Rivers, the Brazil Current boundary is clearly visible from 32°S to 38°S in Figure 27. Farther south, scattered cloud decks obscured the current boundary. Temperatures of 289°K and 281°K can be derived from Figure 28 as average surface temperatures of the Brazil current and the Falkland Current, respectively. After addition of the corrections, discussed earlier, these temperatures are in good agreement with climatological averages for August in this sea region (Hydrographic Office, 1954).

On the following day, August 17, 1966, this ocean current boundary was seen by the infrared radiometer between 30°S and 44°S (Figure 29), i.e., over a much greater area. The northern

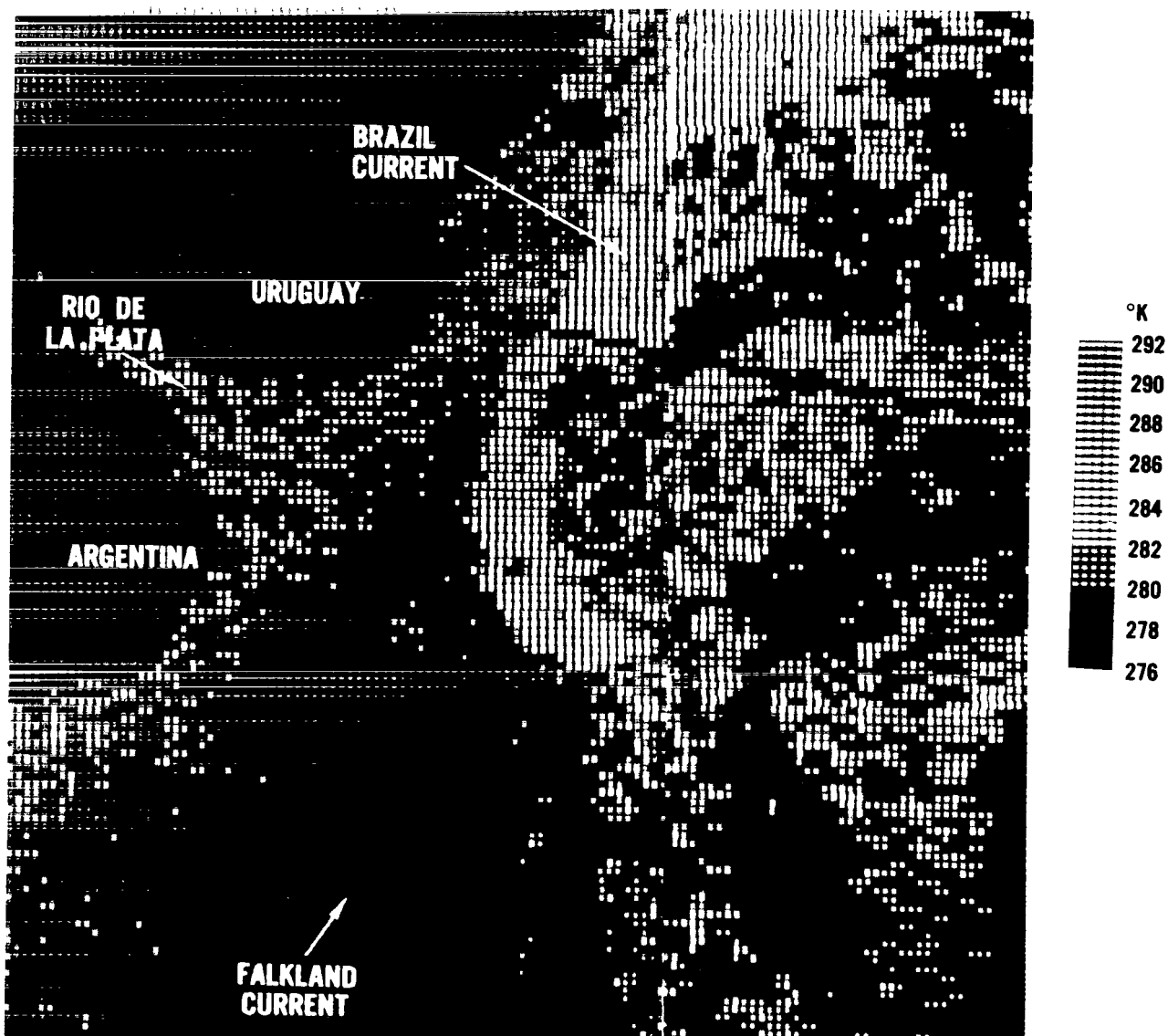


Figure 28—Digital color print of computer grid print map of Nimbus II HRIR measurements on August 16, 1966, 0245 GMT (orbit 1235), over the Atlantic coast of South America. Oscillatory noise was removed from the data. Colors are separated in steps of 2°K.

parts, which are seen on both consecutive days, are a good example of the repeatability of the observation method.

The equivalent black body temperature over the Falkland Current in the lower part of the figure is around 280°K; a steady, slight increase can be noticed toward the north in Figure 30, where 282°K can be derived, on the average, for the northern part of the Falkland Current. The Brazil Current, on the other hand, is characterized mainly by 288° to 290°K. An average temperature contrast of 5.4°K over a mean distance of 24 kilometers can be derived along the inshore edge of the

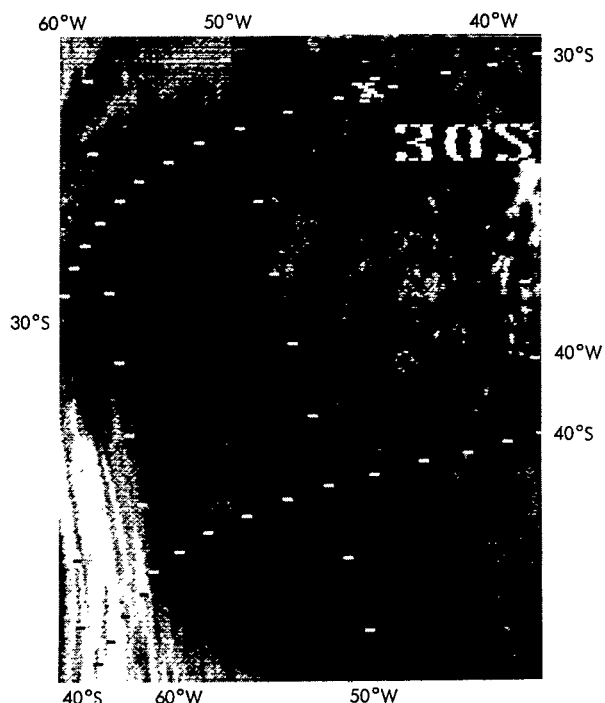


Figure 29—Photofacsimile of Nimbus II HRIR nighttime measurements on August 17, 1966, 0210 GMT (orbit 1248), over the South Atlantic Ocean.

the inshore edge of the Gulf Stream and represents one of the outstanding features in the sea surface temperature distribution.

The Oyashio-Kuroshio Region

The Oyashio-Kuroshio boundary was seen in the Nimbus II HRIR data in a number of cases. Measurements taken on October 6 and 7, 1966 over this region were selected for this presentation because of the characteristic thermal structure exhibited in the area of interference between the two ocean currents. Large parts of northern Japan and the surrounding seas had clear skies on October 7, 1966. Contrary to the examples presented earlier, a number of interesting features, not only in connection with the main current boundaries but also within the main water boundaries themselves, can be observed in the temperature pattern exhibited by the photographic display of the infrared measurements (Figure 33). Most prominent is the temperature contrast between the cold land and warmer ocean waters near midnight. Within the ocean areas, a striking temperature contrast can be seen between the sea regions on both sides of the Kuril Chain. According to the season, the Okhotsk Sea is actually still warmer than the Oyashio flowing southwestwardly east of the Kuril Islands. Very obviously the chain of islands prevents a strong mixing of water bodies of different temperatures. Farther south, the transition from the cold Oyashio waters toward the warmer Kuroshio seems to take place in two distinct steps. A sharp line of temperature contrast can be

Brazil Current between 32° and 40°S for this day. At certain locations, this difference is as high as 10°K, according to Figure 30. Another example for the clear definition of the inshore edge of the Brazil Current is given in Figure 31 by the reproduction of an original analog record of a horizon-to-horizon scan across the current boundary on August 17, 1966. Instrumental noise is a very striking feature in this analog record, but the temperature contrasts visible in the photofacsimile display (bottom of Figure 30) can be identified easily. The numerical filter (developed by McMillin, 1969 to remove the predominant 200-Hz oscillatory noise component of the digitized data) was used on a section of the same scan and is presented in Figure 32. Here the current boundary clearly stands out as a temperature step of almost 10°K.

These sporadic observations indicate that the Brazil and Falkland Current boundary, which is part of the Subtropical Convergence in the South Atlantic Ocean, is as sharply defined as

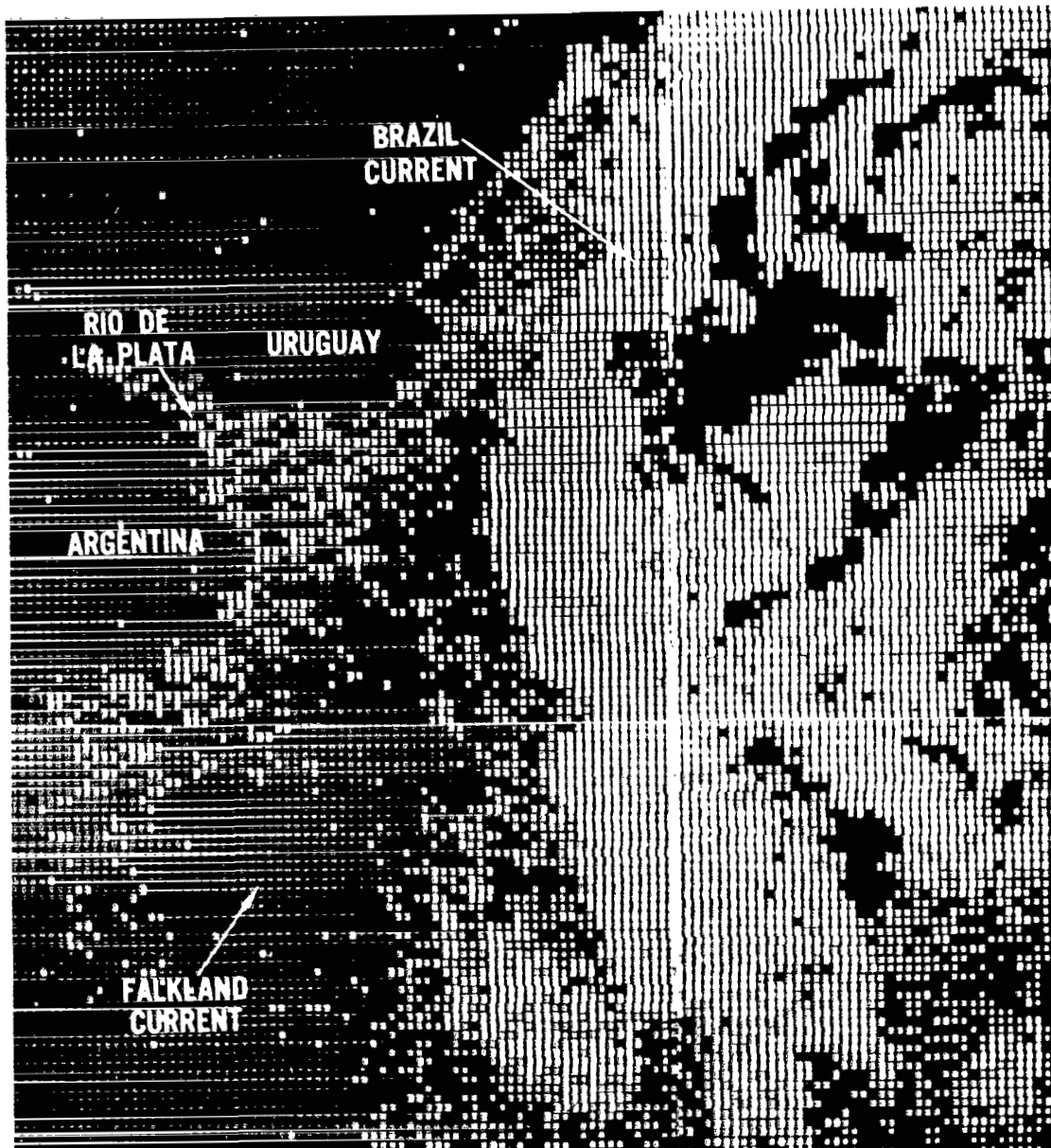


Figure 30—Digital color print of computer grid print map of Nimbus II HRIR measurements on August 17, 1966, 0210 GMT (orbit 1248), over the South Atlantic Ocean. Colors are separated in 2°K steps. Oscillatory noise has been removed from the data.

seen near 41°N; a second one, which seems to represent the northern edge of the Kuroshio itself, is very pronounced somewhat south of 40°N. From Figure 34 it can be seen that the equivalent black body temperatures over the Kuroshio were near 298°K, in the transition zone around 292°K,

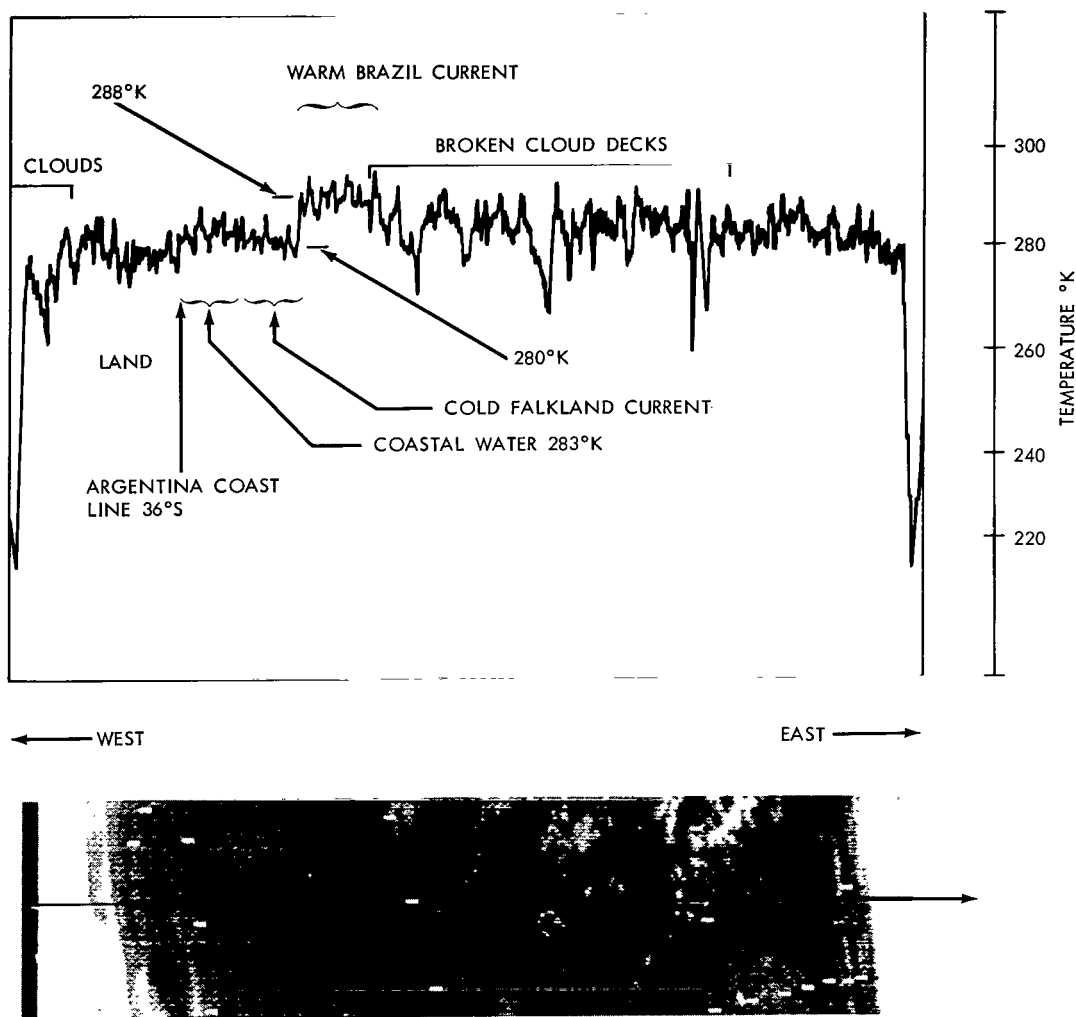


Figure 31—Example of an analog record of an individual scan line of Nimbus II HRIR nighttime (orbit 1248) data taken on August 17, 1966 at 02^h11^m42^s GMT across Argentina and the South Atlantic Ocean. The photofacsimile underneath indicates the exact location of the scan line.

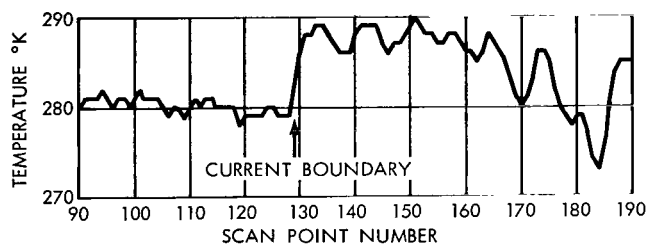


Figure 32—Section of the Nimbus II HRIR analog record reproduced in Figure 31 after digitization and application of a numerical filter to remove oscillatory noise.

and about 286°K in the southern parts of the Oyashio. Because of the possibility of some cloud contamination by perhaps thin cirrus or small convection clouds not resolved by the HRIR instrument, the observations on the preceding day were inspected for the reproducibility of the observed patterns. Figures 35 and 36 show these observations. Although a stronger cloud interference existed on October 6, 1966,

several of the characteristic patterns seen on the next day could be identified. Figure 37 schematically indicates the most prominent structural features repeated in both sets of data. From this, it is obvious that the two boundaries observed are really phenomena in the sea surface temperature distribution. No conclusions on the history or dynamics of this dual boundary between the Oyashio and the Kuroshio can be drawn from these observations yet, but infrared data taken 1 month later over the same region (Figure 38) indicate the persistence of a very complex thermal structure of the Oyashio-Kuroshio interface.

The Agulhas Current

The Agulhas Current is a warm-water current flowing southwestward along the east coast of South Africa and, according to textbooks (Defant, 1961; Pickard, 1964), splitting near 33°S into a weaker branch flowing around South Africa into the South Atlantic Ocean and a stronger branch turning south and merging into the southern Subtropical Convergence near 40°S. Sharp temperature discontinuities within this ocean current were reported by radiometric measurements from aircraft off Durban, South Africa (Harris and Stavropoulos, 1967), but no specifically sharp current boundaries such as those associated with other currents are shown in standard sea surface current maps (Defant, 1961).

The Nimbus II HRIR data contain a good example, with sufficiently reduced cloudiness, that permits the observation of this particular sea region. The infrared photograph of September 19, 1966, reproduced in Figure 39, shows a distinct sea surface temperature discontinuity from about 33.5°S, 27°E to approximately 38°S, 20°E. This line seems to represent the meandering western edge of the Agulhas Current. Over the warmer water, equivalent black body temperatures of 292° to 294°K were recorded, corresponding to sea surface temperatures around 298°K (after correction); the corresponding values over the colder water were 285°K (T_{BB}) and 291°K (corrected temperature). However, as the pictorial display indicates cloud bands were still contaminating the area to some extent; thus these temperatures may be biased toward lower values. These measurements agree satisfactorily with climatic data.

This example proves that structural features of the Agulhas Current can be detected and studied by observations from satellite altitudes. The sharpness of the temperature contrast found

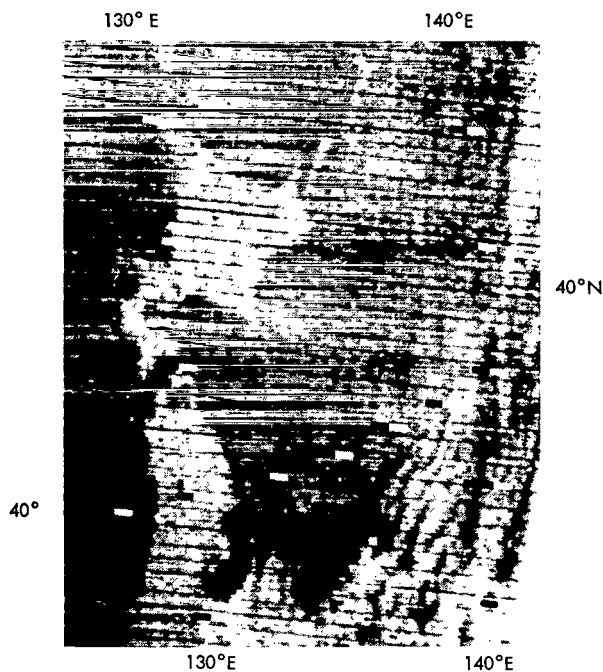


Figure 33—Photofacsimile of Nimbus II HRIR nighttime measurements on October 6, 1966, 1500 GMT (orbit 1921), near Japan.

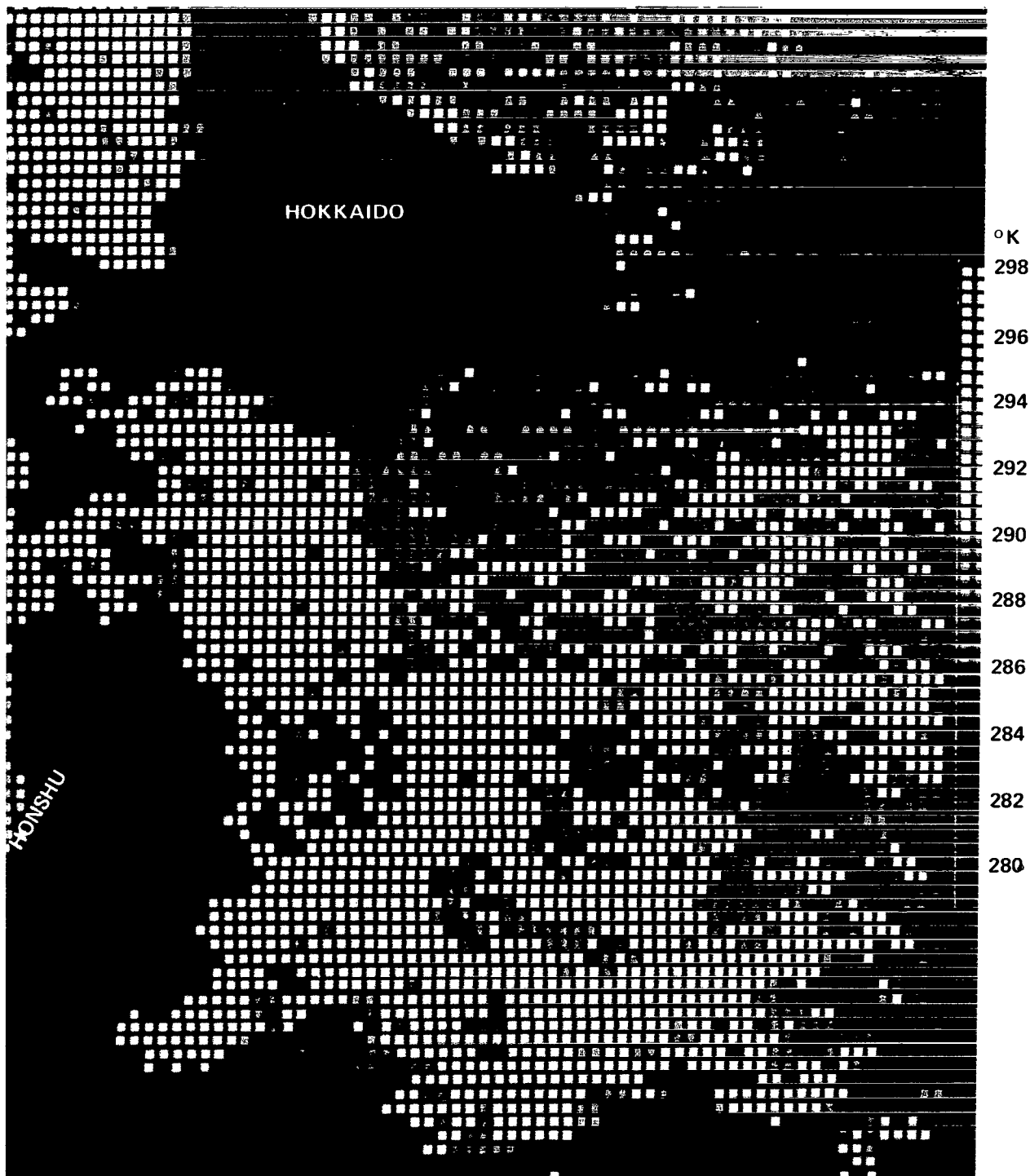


Figure 34—Digital color print of computer grid print map of Nimbus II HRIR nighttime measurements on October 6, 1966, 1500 GMT (orbit 1921), near Japan. Oscillatory noise has been removed from these data. The color steps are equivalent to 2°K temperature intervals.

in this case suggests the existence of a more strongly defined western boundary of the Agulhas current than was expected before. The temperature contrast, indicated by the high resolution infrared measurements of Nimbus, at least in the present case, seems to be as significant as the temperature discontinuities found along the Gulf Stream and Brazil Current boundaries.

CONCLUSIONS

Results from various meteorological satellites suggest many possibilities for using orbiting platforms for oceanographic purposes. This paper presented a survey on the presently available observation techniques and data in sensing sea surface parameters from satellite altitude.

Inference of sea surface temperature patterns from meteorological satellite cloud photography seems to be a promising field for further investigation. The examples given show an obvious correlation between certain sea surface temperature discontinuities and the induced cloud patterns; however, detailed and more quantitative studies in conjunction with ship or airplane observations for ground confirmation are necessary in order to establish a reliable analysis method under cloudy conditions.

In the case of clear skies, infrared measurements of high spatial resolution in one of the atmospheric windows present a second method of deriving sea surface structural features from space. In the 3- to 4-micron window, the Nimbus II HRIR experiment acquired a sizeable quantity of data showing sea surface temperature features, sensed under daytime and nighttime conditions. However, in this near-infrared window, reflected sunlight does not permit the derivation of quantitative sea surface temperature data during daytime. Nighttime observations furnish quantitative information not only on the location of certain ocean current boundaries, but also on the sea surface temperature distribution. Therefore, it would be desirable to change to the 8- to 12-micron window, which is not affected by solar radiation, but lies entirely within the spectral range of thermal radiation of the earth-atmosphere system. Also it would be desirable, under daytime conditions, to have simultaneous, supplemental information on the cloud distribution from a second radiometer channel in the visible spectrum, thus permitting a more accurate interpretation of the infrared measurements in terms of sea surface temperature. During nighttime, no supplemental cloud observation is available yet, although observations in the visible airglow bands from the OGO-4

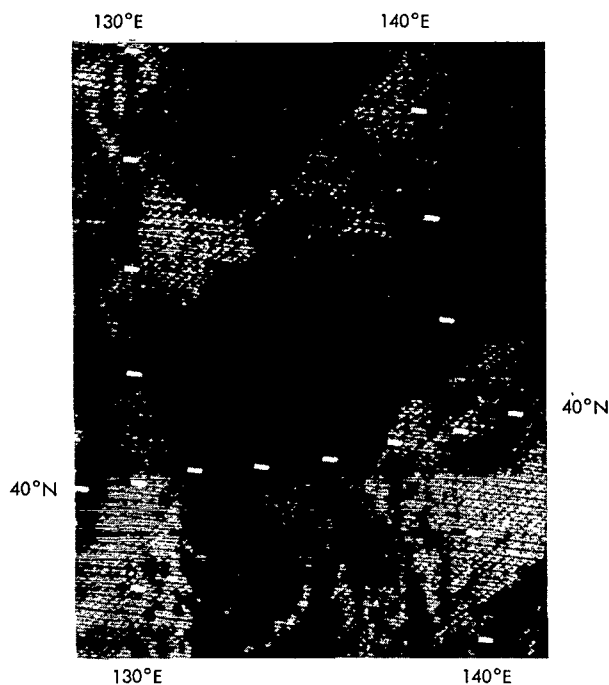


Figure 35—Photofacsimile of Nimbus II HRIR nighttime measurements on October 7, 1966, 1430 GMT (orbit 1934), near Japan.

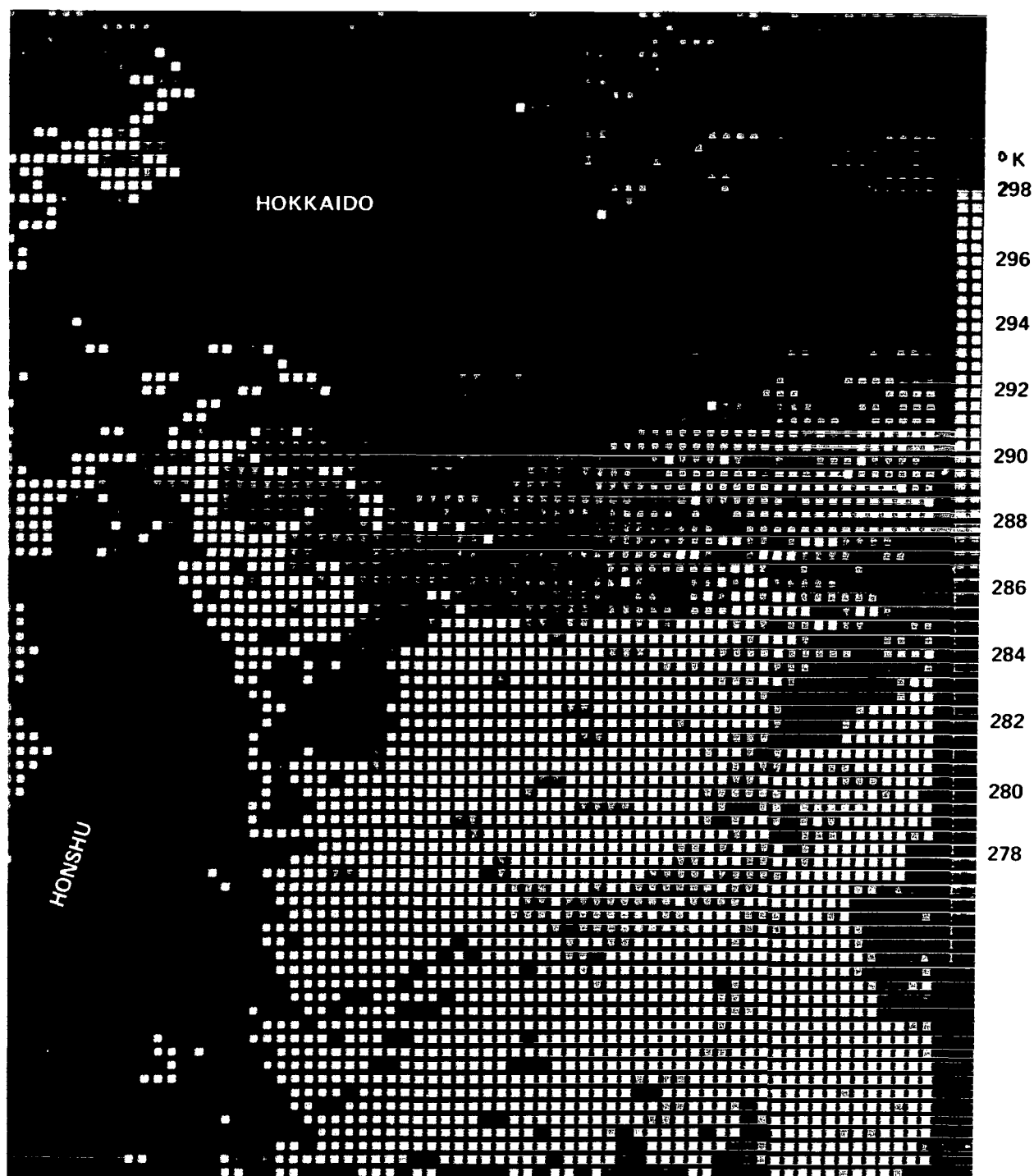


Figure 36—Digital color print of computer grid print map of Nimbus II HRIR nighttime measurements on October 7, 1966, 1430 GMT (orbit 1934), near Japan. Oscillatory noise has been removed from these data. The color steps are equivalent to 2°K temperature intervals.

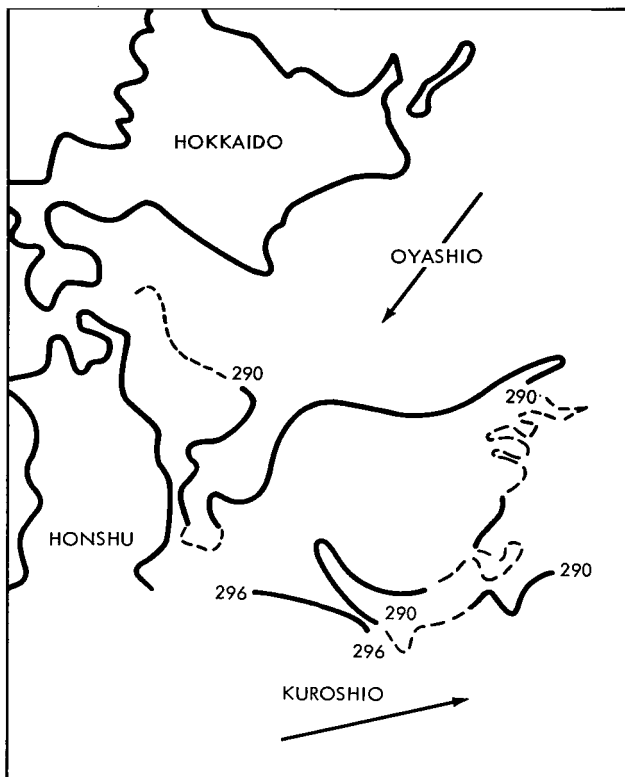


Figure 37—The most significant features in the Nimbus II HRIR nighttime data near Japan which were repeated on October 6 and 7, 1966, representing landmarks and certain temperature discontinuities in the Oyashio-Kuroshio mixing region.

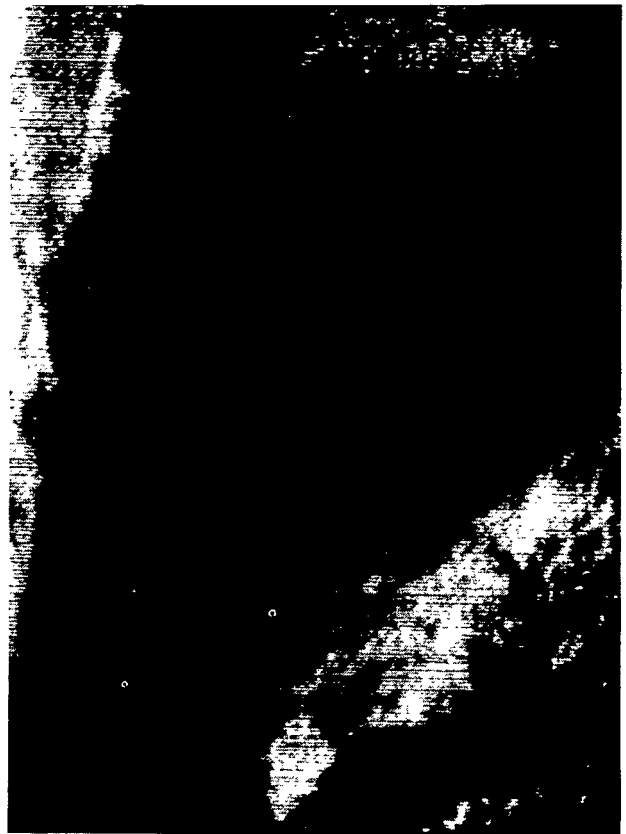


Figure 38—Photofacsimile of Nimbus II HRIR nighttime measurements on November 5, 1966, 1420 GMT (orbit 2320), near Japan.

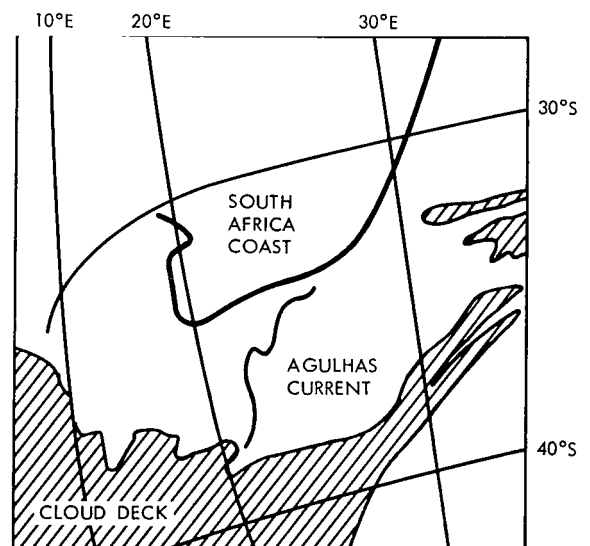
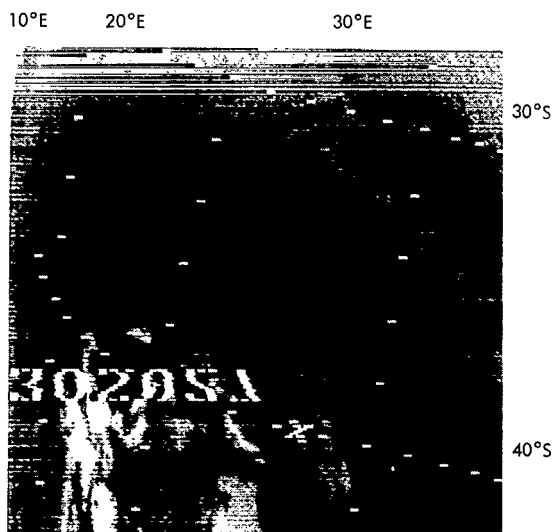


Figure 39—Photofacsimile and schematic analysis of Nimbus II HRIR nighttime measurements on September 19, 1966, 2130 GMT (orbit 1698), near South Africa.

satellite (Warnecke et al., 1968) and the development of a HRIR system to be flown on the ATS-F satellite offer promising possibilities for future research.

Before techniques in other spectral regions such as passive microwaves are explored fully and developed, quantitative information on sea surface temperature by infrared radiometry will be restricted to clear regions. However, fairly useful sea surface data coverage can be achieved if measurements of clear areas taken over a period of several (perhaps 5 to 7) days are composed. This approach should be possible because of the 12-hour frequency of measurements at a certain location by one near-earth satellite and the relatively fast motion of cloud systems compared with the normally observed high persistence of sea surface temperature patterns within periods of several days.

The examples presented of remote detection of sea surface temperature and ocean current characteristics, taken from satellite observations which were originally designed for meteorological purposes only, demonstrate that existing techniques are suitable, after some minor modifications, to establish a satellite-borne, global oceanographic observation system that will open a new dimension of oceanographic research and application.

ACKNOWLEDGMENTS

The authors gratefully acknowledge the interest in, and support of, this work by Mr. John Wilkerson, U. S. Naval Oceanographic Office, Washington, D. C. in supplying radiometric sea surface temperature measurements from research aircraft; by Dr. James R. Smith, Research Triangle Institute, North Carolina, for furnishing the EASTWARD sea surface temperature observations; by Allied Research Associates, Inc. for the production of digital color prints presented in this paper; and by Messrs. Virgil G. Kunde and William R. Bandeen, Goddard Space Flight Center, and Major Earl R. Kreins, USAF, Air Weather Service, for their helpful suggestions.

Goddard Space Flight Center
National Aeronautics and Space Administration
Greenbelt, Maryland, October 1, 1968
160-44-03-96-51

REFERENCES

- Allison, L. J., Foshee, L. L., Warnecke, G., and Wilkerson, J. C., "An Analysis of the North Wall of the Gulf Stream Utilizing Nimbus II High Resolution Infrared Measurements," paper presented at the 48th meeting of the American Geophysical Union on April 17, 1967 in Washington, D. C.
- Allison, L. J., and Kennedy, J. S., "An Evaluation of Sea Surface Temperature as Measured by the Nimbus I High Resolution Infrared Radiometer," NASA Technical Note TN D-4078, Nov. 1967.

- Bandeem, W. R., "Experimental Approaches to Remote Atmospheric Probing in the Infrared from Satellites," Goddard Space Flight Center, Greenbelt, Md., Doc. No. X-622-68-146, pp. 50, May 1968.
- Bramson, M. A., Zel'manovich, I. L., and Kuleshova, G. I., "Izluchatel'naya sposobnost vody v infrakrasnoy oblasti spektra, Trudy Glavnoy Geofizicheskoy Observatorii imeni A.I. Voyekova," No. 152, pp. 31-67, 1964 ("The Emissive Power of Water in the Infrared Region of the Spectrum," NASA Technical Translation TT-F-319, 1965).
- Clark, H. L., "Some Problems Associated With Airborne Radiometry of the Sea," *Applied Optics*, Vol. 6: 2151-2157, 1967.
- Clark, J., "Techniques for Infrared Survey of Sea Temperature," U. S. Department of the Interior, Bureau of Sport Fisheries and Wildlife, Bureau Circular No. 202, pp. 142, 1964.
- Defant, A., "Physical Oceanography," Vol. 1, Oxford, London, New York, Paris, Pergamon Press, 1961.
- Ewing, G. C., and McAlister, E. D., "On the Thermal Boundary Layer of the Ocean," *Science*, Vol. 131: 1374-76, 1960.
- Ewing, G. C., Editor, "Oceanography from Space," Woodshole Oceanographic Institution, Ref. No. 65-10, pp. 469, April 1965.
- Fuglister, F. C., and Worthington, L. V., "Some Results of a Multiple Ship Survey of the Gulf Stream," *Tellus*, (3):1-14, 1951.
- Fujita, T., and Bandeen, W. R., "Resolution of the Nimbus High Resolution Infrared Radiometer," *J. Applied Meteorol.*, Vol. 4: 492-503, August 1965.
- Goldberg, I. L., Foshee, L., Nordberg, W., and Catoe, C. E., "Nimbus High Resolution Infrared Measurements," Third Symposium on Remote Sensing of Environment, The University of Michigan, pp. 141-151, October 14-16, 1964.
- Goody, R. M., "Atmospheric Radiation," Oxford, Clarendon Press, 1964.
- Greaves, J. R., Willand, J. H., and Chang, D. T., "Observation of Sea Surface Temperature Patterns and Their Synoptic Changes Through Optimal Processing of Nimbus II Data," NASA Final Report, Contract No. NASW-1651, Sept. 1968.
- Harris, T. F. W., and Stavropoulos, C. C., "Some Experience with a Radiation Thermometer over the Agulhas Current," *The South African J. of Science*, 63(4):132-136, April 1967.
- Hydrographic Office, United States Navy, "World Atlas of Sea Surface Temperatures," H.O. Publication No. 225, Second Edition, Reprint Washington, D. C. 1954.
- Kunde, V. G., "Theoretical Relationships between Equivalent Blackbody Temperatures and Surface Temperature Measured by the Nimbus High Resolution Infrared Radiometer," NASA Special Publication SP-89, pp. 23-36, Dec. 1965.

- LaViolette, P. E., and Chabot, P. L., "Nimbus II Satellite Sea Surface Temperatures versus Historical Data in a Selected Region: A Comparative Study," *Deep Sea Research*, No. 5: 617-622, October 1968.
- McMillin, L. M., "A Procedure to Eliminate Periodic Noise Found in Nimbus II High Resolution Infrared Radiometer Measurements," NASA Contractor Report (to be published in 1969).
- National Council on Marine Resources and Engineering Development, "United States Activities in Spacecraft Oceanography," U. S. Govt. Printing Office, Washington, D. C., 1967.
- Nimbus Project, "Nimbus II Users' Guide," Goddard Space Flight Center, Greenbelt, Maryland, 1966a.
- Nimbus Project, "The Nimbus II Data Catalog," Vol. 1-5, Goddard Space Flight Center, Greenbelt, Maryland, 1966b.
- Nimbus Project, "The Nimbus II High Resolution Infrared Data World Montage Catalog," Goddard Space Flight Center, Greenbelt, Maryland, 1967.
- Nordberg, W., and Samuelson, R. E., "Terrestrial Features Observed by the High Resolution Infrared Radiometer," NASA Special Publication SP-89, pp. 37-46, Dec. 1965.
- Pickard, G. L., "Descriptive Physical Oceanography," pp. 199, New York: The MacMillan Company, 1964.
- Rao, Krishna, P., "Sea Surface Temperature Measurements From Satellites," *Mariners Weather Log*, Vol. 12(5):152-154, Sept. 1968.
- Stommel, H. M., Von Arx, W. S., Parson, D., and Richardson, W. S., "Rapid Aerial Survey of Gulf Stream with Camera and Radiation Thermometer," *Science*, 117: 639-640, 1953.
- Stommel, H., "The Gulf Stream, A Physical and Dynamical Description," Second Edition, pp. 248, University of California Press and Cambridge University Press, 1965.
- U. S. Naval Oceanographic Office, "Monthly Summary, The Gulf Stream," Vol. 1, No. 8, Publication 16782-GS, Washington, D. C., Aug. 1966.
- U. S. Naval Oceanographic Office, "Monthly Summary, The Gulf Stream," Vol. 2, No. 1, Publication 16782-GS, Washington, D. C., Jan. 1967.
- Wark, D. Q., Yamamoto, G., and Lienisch, J. H., "Methods of Estimating Infrared Flux and Surface Temperatures from Meteorological Satellites," *J. Atm. Sciences*, 19(5):369-384, Sept. 1962.
- Warnecke, G., Allison, L. J., and Foshee, L. L., "Observations of Sea Surface Temperature and Ocean Currents from Nimbus II," *Space Research VIII*, Amsterdam: North-Holland Publ. Co., 1968 [also: Goddard Space Flight Center, Greenbelt, Md., Doc. No. X-622-67-435, Aug. 1967].

- Warnecke, G., Reed, E. I., Fowler, W. B., Kreins, E. R., Allison, L. J., and Blamont, J. E.,
"Meteorological Results from Multispectral Photometry In Airglow Bands by the OGO-4
Satellite, Goddard Space Flight Center, Greenbelt, Md., Doc. No. X-622-68-267, pp. 28, July 1968.
- Wilkerson, J. C., "Airborne Oceanography," *Geo-Marine Technology*, 2(8):9-15, 1966.
- Wilkerson, J. C., "The Gulf Stream from Space," *Oceanus*, XIII (2 & 3): 1-8, June 1967.

NATIONAL AERONAUTICS AND SPACE ADMINISTRATION

WASHINGTON, D. C. 20546

OFFICIAL BUSINESS

FIRST CLASS MAIL



POSTAGE AND FEES PAID
NATIONAL AERONAUTICS AND
SPACE ADMINISTRATION

01U 001 38 51 3DS 69363 00903
AIR FORCE WEAPONS LABORATORY /WLOL/
KIRTLAND AFB, NEW MEXICO 87117

ATT E. LOU BOWMAN, CHIEF, TECH. LIBRARY

POSTMASTER: If Undeliverable (Section 158
Postal Manual) Do Not Return

"The aeronautical and space activities of the United States shall be conducted so as to contribute . . . to the expansion of human knowledge of phenomena in the atmosphere and space. The Administration shall provide for the widest practicable and appropriate dissemination of information concerning its activities and the results thereof."

— NATIONAL AERONAUTICS AND SPACE ACT OF 1958

NASA SCIENTIFIC AND TECHNICAL PUBLICATIONS

TECHNICAL REPORTS: Scientific and technical information considered important, complete, and a lasting contribution to existing knowledge.

TECHNICAL NOTES: Information less broad in scope but nevertheless of importance as a contribution to existing knowledge.

TECHNICAL MEMORANDUMS:
Information receiving limited distribution because of preliminary data, security classification, or other reasons.

CONTRACTOR REPORTS: Scientific and technical information generated under a NASA contract or grant and considered an important contribution to existing knowledge.

TECHNICAL TRANSLATIONS: Information published in a foreign language considered to merit NASA distribution in English.

SPECIAL PUBLICATIONS: Information derived from or of value to NASA activities. Publications include conference proceedings, monographs, data compilations, handbooks, sourcebooks, and special bibliographies.

TECHNOLOGY UTILIZATION PUBLICATIONS: Information on technology used by NASA that may be of particular interest in commercial and other non-aerospace applications. Publications include Tech Briefs, Technology Utilization Reports and Notes, and Technology Surveys.

Details on the availability of these publications may be obtained from:

SCIENTIFIC AND TECHNICAL INFORMATION DIVISION
NATIONAL AERONAUTICS AND SPACE ADMINISTRATION
Washington, D.C. 20546